Evaluation of novel 3D-printed monolithic adsorbers against conventional chromatography columns for the purification of c-phycocyanin from Spirulina

Evaluation of novel 3D-printed monolithic adsorbers against conventional chromatography columns for the purification of c-phycocyanin from Spirulina

Livia C T Scorza[1], Ursula Simon[2], Martin Wear[3], Alex Zouliatis[4], Simone Dimartino[2], Alistair J McCormick[1,†]

[1] SynthSys & Institute of Molecular Plant Sciences, School of Biological Sciences, University of Edinburgh, Edinburgh, EH9 3BF, UK

[2]Institute for Bioengineering, School of Engineering, University of Edinburgh, Edinburgh, EH9 3DW, UK

[3]The Edinburgh Protein Purification Facility, University of Edinburgh, Edinburgh, EH9 3JR, UK

[4]ScotBio, BioCity Scotland, Motherwell, ML1 5UH, UK

[†] Corresponding author

Article type: Research

Authors:	Emails:	ORCID:
Livia C T Scorza	scorza.livia@gmail.com	0000-0002-0145-3592
Ursula Simon	u.simon@ed.ac.uk	
Martin Wear	martin.wear@ed.ac.uk	0000-0003-2208-2986
Alex Zouliatis	alex@scotbio.com	
Simone Dimartino	simone.dimartino@ed.ac.uk	0000-0002-9695-1278
Alistair McCormick	alistair.mccormick@ed.ac.uk	0000-0002-7255-872X

[†]corresponding author:
Dr Alistair J. McCormick
Daniel Rutherford Building, Institute of Molecular Plant Sciences
School of Biological Sciences, University of Edinburgh
The King's Buildings, EH9 3BF Phone: +44 (0)1316505316

Abstract

Extraction and purification of high-grade phycobiliproteins is a multistep process that typically involves costly chromatographic separation techniques. 3D printing approaches and materials can now be tailored to fabricate low-cost anion exchange monolithic adsorbers for chromatography. In this work, a new printing formulation was used to produce monolithic discs with quaternary amine functionality. The 3D-printed discs were tested for the purification of the phycobiliproteins c-phycocyanin and allophycocyanin from extracts of the cyanobacterium *Arthrospira platensis* (Spirulina). Analytical grade c-phycocyanin with 41 ± 7 % recovery was obtained with the 3D-printed discs in a single step. The 3D-printed discs also demonstrated similar or higher separation properties when compared with commercial Q-Sepharose and commercial monolithic discs. Reproducibility tests showed that the fabrication of the 3D-printed discs was robust and potentially scalable for industry-scale purification. Overall, the operative flexibility, robustness and separation performance of the 3D-printed discs demonstrated the promising potential of monolithic adsorbers for the separation of a wide range of biomolecules.

Keywords: allophycocyanin, anion exchange, Arthrospira platensis, disc, downstream processing, phycobilisome.

1. Introduction

Microalgae are a metabolically diverse group of photosynthetic organisms that can be used to sustainably produce commodity biochemicals and sequester carbon dioxide (CO_2) [1,2]. An increasing demand for naturally sourced food additives, cosmetic and health products has driven rapid growth in the microalgal biotechnology industry [3,4], which has a forecasted compound annual growth rate of 4.6% from 2017-2026 [5]. However, optimising downstream processes, including product extraction, purification and yield, remains a key challenge for improving commercial viability [6].

Arthrospira platensis (commonly known as Spirulina) is a cyanobacterial species that has been mass cultivated at large scales with sustained commercial success for several decades [7]. Important products extracted from Spirulina include the blue phycobiliproteins c-phycocyanin (CPC) and allophycocyanin (APC). CPC and APC are both components of the phycobilisome light harvesting complex with absorbance peaks at 620 and 652 nm, respectively. CPC, in particular, is considered a high value product due to the current widespread demand for natural blue colourants [8]. The purity of CPC extracts is typically estimated by spectrophotometry using the ratio of the CPC absorbance peak vs. total protein (i.e., A620/A280) [9]. The purity ratio is generally classified as food grade (A620/A280 > 0.7) up to analytical grade (A620/A280 > 4) [10–12], with the market price of CPC increasing with its purity grade.

Achieving high purities for CPC remains a costly process that involves several processing steps [9]. Cell disruption for crude extraction of phycobiliproteins from Spirulina biomass can be done using a variety of methods, including freezing and thawing, homogenisation [10,13,14], or more expensive approaches such as supercritical CO_2 extraction [15]. Purification of CPC from the crude lysates generally requires appropriate extraction buffers (e.g., in terms of pH and ionic strength), precipitation using ammonium sulphate, followed by dialysis and then one or more chromatography methods, such as expanded bed absorption

chromatography (EBAC), gel filtration or packed bed ion-exchange chromatography [10,12–14,16–19]. Large scale production of concentrated CPC solutions can be achieved with EBAC, but further purification (e.g. ~~.~~., using packed bed anion exchange chromatography) is necessary to achieve higher purity ratios (i.e. ~~.~~., towards analytical grade) and remove APC [18,20]. Reducing the costs and number of unit operations involved in CPC recovery and purification are important industry goals.

The growing availability of open source resources in the research community has accelerated the 'in-house' manufacture of bespoke scientific equipment and materials at a lower cost and with higher specifications [21]. 3D printing has emerged as an important tool in this process, due to the relatively low costs of 3D printers, the increasing improvements in resolution and robustness, and the wide range of input materials that can be used [22]. Recent work has demonstrated the suitability of 3D printing for the fabrication of chromatography columns, including the creation of stationary phases with precisely ordered structures [23–25], together with column housing, flow distributors and connectors in one single fabrication step [26–28]. 3D printing allows the fabrication of tailored devices for individual separation challenges, which can enhance the purification efficiency and reduce costs compared to standard commercial columns [29]. The wide-ranging potential of 3D-printed chromatography columns has been described in detail in two recent reviews by Salmean and Dimartino [30] and Fee [29]. In particular, 3D printing of anion-exchange ~~(AEX)~~ chromatography columns has the potential to provide specialised and highly efficient separations at a much reduced cost compared to standard commercial columns [30,31]. However, the technology is currently constrained by the limited availability of 3D printing materials that present suitable ligands for protein adsorption.

Chemical functionality for chromatography (e.g. ~~AEX~~., anion-exchange) can be introduced to 3D printed materials by adding bifunctional monomers bearing in their molecular structure

both the desired chromatographic ligand as well as a chemical group that can undergo polymerisation. Previously, Simon and Dimartino [31] succeeded in 3D-printing quaternary amine (QA) functionalised columns in a single preparation step that demonstrated protein binding capacities in line or exceeding commercial available materials. More recently, Simon et al. [32] have demonstrated the use of a 3D-printed ~~AEX~~anion-exchange monolithic bed with Schoen gyroid morphology for the purification of CPC from crude Spirulina extracts. Despite the high protein binding capacity of this material, CPC and APC could not be fully resolved as they eluted together.

In this work, monolithic discs with QA functionality were 3D-printed using a novel material formulation based on methacrylates. The material was optimised in terms of chemical stability, which allowed cleaning-in-place ~~(CIP)~~ procedures with sodium hydroxide (NaOH) to ensure sanitised conditions over consecutive runs. Furthermore, the porous morphology of the material facilitated an increase in mass transfer and column efficiency compared to those previously reported [31,32]. The 3D-printed discs were then tested using step elution experiments for the separation of CPC and APC from clarified phycobiliprotein~~-~~-enriched Spirulina extracts. Our results were compared against equivalent commercial strong ~~AEX~~anion-exchange columns also based on the QA functionality, namely a traditionally resin packed Q-Sepharose column and a monolithic CIM® QA disc column. To demonstrate the potential for industry implementation, the robustness of the 3D printing methods and materials were assessed over repeat cycles and for different column batches. Finally, the elution protocol was optimised to improve CPC recovery from this operation.

2. Materials and methods

2.1 Materials

Phenyl bis(2,4,6-trimethylbenzoyl)-phosphine oxide (Omnirad 819, formerly called Irgacure 819) was donated by IGM resins (Waalwijk, The Netherlands). Tinuvin 326 was donated by BASF (Ludwigshafen, Germany). 1-Dodecanol (98%), 2-(Methacryloyloxy)ethyltrimethylammonium chloride 72% aqueous solution), cyclohexanol (98% (v/v)) and ethanol (99.8% (v/v)) were purchased from Fisher Scientific (Waltham, MA, USA). Ethylene glycol dimethacrylate (EDMA, SR206) was donated from Sartomer Europe (Colombes Cedex, France). Analytical grade sodium phosphate (monobasic, dihydrate; $NaH_2PO_4 \cdot 2H_20$) and sodium chloride (NaCl) were purchased from Fisher Scientific (Waltham, MA, USA). All chemicals were used as received.

2.2 Column 3D printing

The material for 3D printing was prepared by dissolving 1 g of the radical photoinitiator Omnirad 819 and 0.1 g of the photoabsorber Tinuvin 326 in a 100 ml mixture of methacrylate monomers (16% (v/v) EDMA, 12% (v/v) [2-methacryloxy)ethyl]trimethylammonium chloride (MAETAC) and 12% (v/v) (Hydroxyethyl)methacrylate (HEMA)) and porogenic solvents (48% (v/v) cyclohexanol and 12% (v/v) 1-dodecanol). All formulations were stored at room temperature (RT) in tubes covered in aluminium foil to prevent spontaneous polymerisation and were ultra-sonicated for 10 min prior to 3D printing.

Monolithic QA discs with a diameter of 12 mm were designed and sliced using Netfabb 2019 (Autodesk, San Rafael, CA, USA). 3D printing was performed using a Solflex 350 digital light processing ~~(DLP)~~ printer (W2P Engineering, Vienna, Austria) with a UV-LED at 385 nm. All parts were printed with 50 µm layers using an energy of 40 mJ/cm^2 for the curing of each layer. After printing, the discs were cleaned extensively in 99.8% (v/v) ethanol in three consecutive washes on a roller mixer SRT9D (Stuart, Staffordshire, UK). The discs were then stored in 20% (v/v) ethanol until further use. For the separation experiments, the printed discs

were introduced into polylactic acid ~~(PLA)~~ rings having 12 mm and 15.9 mm inner and outer diameter, respectively and a height of 3 mm (equivalent to a column volume of 340 µl). The ~~PLA~~polylactic acid rings were separately 3D-printed using a fused deposition modelling (FDM) printer (KLONER3D®140, KLONER3D® - Clevertek s.n.c., Florence, Italy) and employing a 1.75 mm ~~PLA~~polylactic acid filament from Rigid.Ink (Wetherby, UK).

2.3 Scanning electron microscopy imaging of 3D-printed monoliths

A Zeiss Crossbeam 550 Focused Ion Beam Scanning Electron Microscopy (~~FIB-SEM)~~ ~~(~~Jena, Germany) with Quorum Technologies PP3010T preparation system (Laughton, UK) was used to analyse the microscopic structure of the 3D-printed monoliths. Monoliths were frozen in liquid nitrogen, freeze fractured, sublimated at -90°C for 60 min and then platinum sputter coated prior to imaging.

2.4 Phycobiliprotein extracts

Phycobiliprotein-enriched extracts from *Arthrospira platensis* biomass were provided by ScotBio (Scotland, UK). The *A. platensis* culture was initially harvested using 22 µm filtration bags to obtain a wet algal biomass, which was then mixed with water to make a 30% (w/v) biomass solution. Four different methods were then used for cell disruption and phycobiliprotein extraction: 1) high-shear homogenisation (HS), 2) freezing and thawing (FT), 3) freezing and thawing followed by mixing (FT+M), and 4) freezing and thawing followed by homogenisation (FT+H~~))~~ [20,33–35]. For HS, the biomass solution was subjected to 15 min of high-shear homogenisation at 15,000 rpm using a rotor-stator (T25 Easy Clean, IKA, Germany). Due to the heat generated by rotor-stator, the biomass solution was kept in an ice-bath during high-shear homogenisation. This was followed by 3 hours of low-shear mixing at 200 rpm at room temperature (RT). For FT, FT+M and FT+H the biomass solution underwent

two cycles of freezing (-18°C for 24 hours) and thawing (4°C for 15 hours). For FT+M the solution was mixed for one hour at 200 rpm at RT after the second cycle. For FT+H the solution was homogenised at 15,000 rpm for 15 min in an ice bath after the second cycle. The four extracts were then clarified by two rounds of centrifugation at 9,000 g for 30 min (Multifuge 3 L-R, Thermo Fisher Scientific, USA). The supernatants of the FT, FT+M and FT+H extracts were filtered through 20-25 µm filter paper (Grade 4, Whatman). All extracts were then filtered through a 5 µm polypropylene membrane filter and finally through a 0.8/0.2 dual PES membrane filter (Polycap HD 36 and Polycap TC 36 capsule filters, respectively, GE Healthcare Lifesciences, USA).

2.5 C-phycocyanin purification

An Äkta Pure 25 chromatography system (GE, USA) equipped with a UV monitor for triple wavelength detection was used to quantify components within the clarified extracts, including total extracted protein, CPC and APC at absorbances of 280, 620 and 652 nm, respectively. Prior to loading, the extracts were diluted in 50 mM NaH_2PO_4 (pH 7.0) and then in 25 mM NaH_2PO_4 (pH 7.0) to reduce the ionic strength of the extracts to that of the equilibration buffer (25 mM NaH_2PO_4 and 20 mM NaCl (pH 7.0)) that had a conductivity of *ca*. 4 mS/cm. The dilution factor was the same for all extracts (6-fold dilution). The diluted extracts were filtered one more time through a 0.22 µm syringe filter (Millex-GP, Merck, Germany). The concentration of CPC in each diluted extract is listed in **Table 1**.

The performance of the 3D-printed discs was compared with a commercial Q Sepharose packed column (HiTrap Q HP® 1 ml) (GE, USA) and a commercial monolithic disc (CIM® QA disc, 0.34 ml column volume, BIA Separations, Ajdovščina, Slovenia). Each column type was tested using the four different types of clarified phycobiliprotein extract (n=4 biological replicates each). All chromatography columns were equilibrated with equilibration buffer prior

to sample loading. A loading of 1 mg of CPC per ml of column volume (CV) was fed to the columns, with total load volume adjusted according to CPC concentration and column volume. The columns were then washed with 5 CVs of equilibration buffer, eluted with a linear NaCl gradient (column dependent) and finally washed with 5 CVs of 1 M NaCl solution. As each column type is characterized by its specific binding properties, elution conditions were tuned to enable recovery of the CPC. For the HiTrap column a 25 CV NaCl gradient from 20 to 200 mM was initially employed. A following step elution with 15 ~~CV~~CVs of 90 mM and 15 ~~CV~~CVs of 120 mM NaCl was carried out to recover CPC and APC, respectively. The CIM® disc was eluted with a 50 CV gradient from 20 to 200 mM NaCl, while step separation was performed with 20 ~~CV~~CVs of 125 mM and 20 ~~CV~~CVs of 170 mM NaCl for CPC and APC elution, respectively. The 3D-printed discs were eluted with a 50 CV gradient from 20 to 500 mM, with step separation performed with 20 ~~CV~~CVs of 200 mM and 20 ~~CV~~CVs of 320 mM NaCl for APC and CPC elution, respectively. New unused 3D-printed discs were used for each phycobiliprotein extract (i.e~~.~~., HS, FT, FT+H and FT+M). All chromatography runs were performed at 8°C and with a flow rate of 1 ml/min for the HiTrap column and 2 ml/min for the monolithic disc columns.

2.6 Robustness of 3D-printed discs for the separation of phycobiliproteins

To test the robustness of the 3D printed discs, in particular the consistency of the separation results over consecutive runs, two unused 3D-printed discs were tested using the phycobiliprotein-enriched ~~extract (~~FT~~)~~ extract over five and thirteen separation cycles, each consisting of sample load, washing with equilibration buffer, step elution and washing with 1 M NaCl (as described in 2.5).

2.7 CPC purity and concentration calculations

The attributes of the initial phycobiliprotein-enriched extracts and the eluted CPC fractions were calculated based on the absorbance at 280 nm (total protein content), 620 nm (CPC) and 652 nm (APC). For the phycobiliprotein-enriched extracts, each sample was loaded into the Äkta Pure 25 chromatography system, bypassing the column. The UNICORN software (GE, USA) was employed to integrate the peaks and estimate the volume of the eluted fractions. The purity of CPC was calculated using the A620/A280 ratio as in [9]. The separation factor of CPC from APC was calculated as the A620/A652 ratio [36]. CPC recovery was calculated as the ratio of the amount of CPC collected in the eluted fractions with respect to the mass of CPC fed to the columns. The concentration of CPC was estimated as proposed by Bennett and Bogorad [37]:

[CPC] (mg/ml) = [A620 - 0.474 (A652)] / 5.34

2.8 UV-VIS absorption spectrum and SDS-PAGE

To further compare the purity and protein composition of the eluted CPC and APC fractions against the initial clarified phycobiliprotein extracts, the UV-VIS absorption spectra were measured, and SDS-PAGE was performed for the initial extracts and purified fractions from all of the three ~~AEX~~anion-exchange columns used. Absorption was measured using a NanoDrop 1000 spectrophotometer (Thermo Fisher Scientific, Waltham, MA, USA). Proteins were separated by SDS-PAGE on a Bolt Bis-Tris Plus gel (Invitrogen, Thermo Fisher Scientific, Waltham, MA, USA) and visualised by staining with Coomassie Brilliant Blue R-250 (BioRad, Hercules, CA, USA).

3. Results and discussion

3.1 Fabrication of the 3D-printed discs

Monolithic discs were 3D-printed using an optimised version of our previously reported acrylate-based QA printing materials (**Fig. 1A**) [31,32]. 3D printing materials are comprised of a complex mixture containing monomers and crosslinkers that form the polymeric network, while a photoinitiator and photoabsorber are used to start and control the polymerisation reaction, respectively, during the printing process [22]. To print fully functional stationary phases for ~~AEX~~anion-exchange chromatography, we introduced porogenic compounds to create pores at the nanometer scale and bifunctional monomers to provide QA ligands. Compared to the previous acrylate-based materials, the new material was solely composed of methacyrylate monomers and crosslinker. This resulted in good alkaline stability that allowed standard ~~CIP~~cleaning-in-place procedures with 1M NaOH. In addition, the ratio of monomer to crosslinker was tuned to 40:60 to create a more open porous network. The resulting 3D-printed monoliths were similar in size and shape to commercial CIM® discs.

After the printing process, the monoliths were extensively cleaned with ethanol to ensure the removal of uncured monomers, porogens, photoinitiator and photoabsorber. During the washing procedure the monoliths changed in appearance from yellow, directly after printing, to white after several washing steps (**Fig. 1A)**. Successful removal of the introduced porogens was demonstrated using SEM, which showed an interconnected globular network (**Fig. 1B**). This morphology is typical for monoliths fabricated using porogens such as cyclohexanol and dodecanol [38,39]. Flow through pores in the order of 1 µm were estimated using SEM images. This corresponded to a four-fold increase in pore size compared to previous 3D-printed QA materials [32], which indicated better pore accessibility and improved diffusional mass transfer. The porous structure of the 3D-printed monolithic discs was also confirmed by a drop in pressure of 3 ± 0.3 bar at a flow rate of 2 mL/min, which is equivalent to a permeability of 3×10^{-15} m^{-2}. These results are in line with other monolithic materials, such as CIM® discs that have a reported permeability of 6 x 10^{-15} to 1 x 10^{-14} m^{-2} [40,41].

To confirm a tight fitting of the 3D-printed monolithic discs within the ~~PLA~~polylactic acid ring and no leakage at the interface (**Fig. 1A**), we performed residence time distribution ~~(RTD)~~ experiments using acetone as non-retained tracer. A first moment of μ_1 = 0.270 ± 0.002 ml was determined for all discs, which demonstrated that the discs had a consistent porous structure and that structural defects had not resulted from the insertion of the discs into the ~~PLA~~polylactic acid rings. In addition, no fronting due to channelling was observed in the ~~RTD~~residence time distribution curves, which further confirmed a tight fit of the discs in their ~~PLA~~polylactic acid casings.

3.2 Comparison of separation and purification of phycobiliproteins

The concentration of CPC, CPC purity and the CPC/APC separation factor for the four phycobiliprotein-enriched extracts are summarised in **Table 1**. Chromatographic runs were performed for all phycobiliprotein extract-column combinations. Separation of CPC and APC was initially carried out with linear NaCl gradients (**Supplementary Fig. S1-S3**). The NaCl concentration at which APC and CPC eluted informed the NaCl concentrations used for subsequent step elution runs (**Supplementary Fig. S4-S6**). For all three columns tested, the flow-through and column wash fractions did not appear to contain significant amounts of APC and CPC. This confirmed that the phycobiliproteins were appropriately adsorbed to all ~~AEX~~anion-exchange resins, whereas most of the soluble protein content in the extracts was not retained and collected in the flow through.

Overall, CPC and APC eluted at lower NaCl concentrations from the HiTrap column (**Fig. 2A**) than from the two monolithic materials **(Fig. 2B, C**). The commercial CIM® QA monolithic disc required 1.4-fold higher NaCl concentration for the recovery of both APC and CPC, while a 1.6- and 3.5-fold increase was necessary for elution of APC and CPC from the custom 3D-printed discs, respectively. The latter result highlighted the stronger protein binding

properties of the new formulation used to make the 3D-printed discs, as the NaCl concentration required for CPC elution with our previous material was similar to that for CIM® QA discs [32]. Our results also indicated differences in the binding interactions of the two phycobiliproteins with the different stationary phases, with stronger binding to the methacrylate-based monolithic discs than the Sepharose backbone of the HiTrap resin.

Interestingly, both commercial columns eluted CPC first followed by APC, whereas the trend was reversed when using the 3D-printed discs. The adsorption and retention properties of a chromatography column are highly dependent on the binding interactions that biomolecules establish with the stationary phases. The observed elution reversal effect indicated the formation of complex interactions between the phycobiliproteins and the 3D-printed discs, possibly due to a combination of ion-exchange and hydrophobic interactions characteristic of multi-modal chromatography [42]. Interactions with the spacer arm employed to link the ion-exchange moieties to the stationary phase could also have influenced the retention characteristics [43]. For example, a relatively short C2 spacer links the QA moieties to the backbone of the 3D-printed discs due to the chemical structure of the bi-functional MAETAC monomer [31]. Thus, any adsorbed biomolecules would be sterically adjacent to the polymeric backbone, which could facilitate additional weak interactions, such as van der Waals and hydrophobic interactions. In contrast, CIM® discs and the beads used in HiTrap columns are manufactured in a 2-step process, where the backbone is first polymerised and cross-linked, followed by ad-hoc immobilization of the Q ligand. While this production method is longer and more complex, it enables higher flexibility of the resulting chemistry and associated protein-ligand interactions.

For each column type, consistent profiles of APC and CPC elution, CPC purity and recovery were observed for all four extracts showed (**Fig. 2D-F**). This indicated that the different harvest and cell disruption methods had a negligible influence on the following purification steps.

Furthermore, similar CPC purities were observed for all three columns, with an average CPC purity of 3.8 ± 0.3, 3.6 ± 0.1 and 4.2 ± 0.3 (mean ± SD; n=4) for the HiTrap column, CIM® disc and 3D-printed disc, respectively (**Fig. 2D**). This corresponds to a 2.6-fold increase in purity compared to the initial extracts. The CPC purity levels obtained with the 3D-printed discs were typically above 4 (i.e., analytical grade [10,11]). The CPC/APC separation factor was also increased, with an average 2-fold increase for the HiTrap column and a 3-fold increase for both the CIM® disc and 3D-printed disc (**Fig. 2E**). The CPC/APC separation factor was above 6.0 for most of the purified CPC extracts, but for FT+M and FT+H extracts separated with the HiTrap column an average CPC/APC separation factor of 4.0 was achieved. These initial step separation protocols were not optimized for CPC recovery, and co-elution of CPC and APC was observed for all columns, with a significant portion of CPC entering the APC-rich fraction. This resulted in average CPC recoveries of 53 ± 3%, 61 ± 6% and 41 ± 7% (mean ± SD; n=4) for the HiTrap column, CIM® disc and 3D-printed disc, respectively (**Fig. 2F**).

Analyses of the UV-VIS absorbance spectra from each of the purified extracts showed expected peaks at 620 nm and 652 nm for CPC- and APC-enriched fractions, respectively (**Fig. 3A**; **Supplementary Fig. S7A**). All APC fractions also had a peak at 620 nm, as a portion of CPC eluted together with APC in all columns tested (**Fig. 2A-C**). The separation of CPC from APC was further confirmed by SDS-PAGE, where separate bands corresponding to the α- and β-subunits of CPC and APC were visualised (**Fig. 3B**; **Supplementary Fig. S7B**). As observed for absorbance measurements, bands for the subunits of CPC were also present in the APC-enriched fractions, whereas the CPC-enriched fraction did not show any appreciable APC content.

Three hypotheses for the observed co-elution of CPC with APC are summarised below. Firstly, residual CPC may be bound to APC by the phycobilisome rod-core linker protein LRC [36,44]. Although phycobilisome linker proteins (including LRC) were found in the more

concentrated phycobiliprotein-enriched extracts, LRC was not observed in the purified extracts (**Supplementary Fig. S7B**). Secondly, unbound CPC in solution can exist in a variety of oligomeric states of different net charge (i.e., monomers, trimers and hexamers) [45], and thus might elute at different NaCl concentrations resulting in overlap with APC. Thirdly, different binding sites on the monolith surface may lead to the formation of multiple complex interactions with the phycobiliproteins, thus altering the elution pattern during the NaCl gradient.

By appropriate optimisation of the elution protocol, it would be possible to obtain a range of different fractions with each having specific CPC purity and CPC/APC levels for different commercial targets (e.g., food up to analytical grade). Furthermore, APC is a co-product with important added value from this manufacturing process, with commercial potential similar to that of CPC [46]. For example, APC is also considered a high value product and has been used as a fluorescent label and a phycobiliprotein-conjugate in research applications [47].

3.3 Robustness of the fabrication protocol and reproducibility of successive separation cycles with the 3D-printed discs

Validation of the robustness of the manufacturing protocols and consistency of the chromatographic performance are extremely important to enable industry implementation of these new materials in manufacturing operations. To test the reproducibility of the fabrication procedure of the 3D-printed discs, five successive separation cycles were performed with two unused discs using the FT phycobiliprotein-enriched extract. The results for the two discs were comparable to each other and provided a preliminary demonstration of the robustness of the 3D printing protocol and materials employed indicating that the fabrication of the 3D-printed discs was highly consistent.

To test the robustness of the 3D printed monolith over consecutive runs, one disc was tested for a further eight cycles, for a total of thirteen cycles. A minor decline in CPC purity and recovery was observed from cycle to cycle, with an average decrease of less than 2% per cycle (**Fig. 4A, C**). While this decrease was practically negligible for two adjacent cycles, it was compounded over several subsequent cycles, which led to a drop in purity and recovery of approximately 20% over the 13 cycles performed. CPC purity declined from an initial value of 4.2 to 3.5, while CPC recovery decreased from approximately 40% in the first cycle to 28% in the thirteenth cycle.

The phycobiliprotein extracts contained a complex mixture of proteins, lipids and metabolites. For the two commercial columns, qualitative changes in appearance similar to those seen for the 3D-printed discs were also observed after repeated runs (e.g. green staining and retention of phycobiliproteins and chlorophyll that could not be removed with a 1 M NaCl wash). Notably, we did not attempt to optimise the washing or cleaning stages for separations using the 3D-printed discs. As such, more appropriate column regeneration steps still need to be developed, for example, employing reverse flow and/or using cleaning buffers such as 6 M guanidine hydrochloride, methanol, isopropanol or 1 M NaOH [48]. Results over repeated cycles also suggested that the CIPcleaning-in-place step should be performed after every five cycles for consistent operation (i.e., when the drop in CPC purity and recovery are limited to within 5% with respect to the first cycle).

The CPC/APC separation factor was fairly constant between cycles (7 ± 0.5; mean ± SD; n=18) and always remained above 5 (**Fig. 4B**), which is in line with previously reported values using conventional AEXanion-exchange columns [16,20]. The observed reproducibility of step elution runs over repeated cycles demonstrated the robustness of the 3D-printed monoliths for chromatographic separations, which should help with future implementation in the process industry.

3.4 Optimisation of c-phycocyanin recovery using 3D-printed discs

In the step separations described in sections 3.2 and 3.3, a significant portion of CPC co-eluted together with APC, thus explaining the low recoveries observed in the CPC-rich fractions (**Fig. 2F**). 3D-printed discs displayed a smaller recovery than the commercial columns, which is in line with the observation that APC eluted first (i.e~~.~~.., in the 200 mM NaCl step) when the column still has a relatively large CPC loading. Yet, the majority of APC eluted in the first half of the 200 mM step (**Fig. 2C**), which suggested that the recovery of CPC from the 3D-printed discs could be improved by either adjusting the duration of the elution steps or by pooling different eluted fractions together. To test this hypothesis, unused 3D-printed discs were tested with the FT phycobiliprotein-enriched extract (an arbitrary choice) using five different approaches:

(1) Step elution as in sections 3.2 and 3.3 (i.e~~.~~.., 20 ~~CV~~CVs at 200 mM NaCl and 20 ~~CV~~CVs at 320 mM NaCl, with CPC collected only from the 320 mM step) (**Fig. 5A**);

(2) Step elution as in (1), but CPC fractions were also collected from the second half of the 200 mM step (**Fig. 5A**);

(3) The length of the 200 mM step was reduced to 10 ~~CV~~CVs, while the 320 mM step was kept at 20 ~~CV~~CVs. CPC was collected only from the 320 mM step (**Fig. 5B**);

(4) The length of the 200 mM step was reduced to 10 ~~CV~~CVs, while the 320 mM step was increased to 30 ~~CV~~CVs. CPC was collected only from the 320 mM step (**Fig. 5C**);

(5) The total recovery of CPC was calculated for both steps of the latter experiment. This was equivalent to collecting fractions from both elution steps in the other elution protocols, and equivalent to a single step elution at 320 mM NaCl.

The recovery of CPC in the first approach was 33%. However, recoveries improved in the subsequent approaches from 48% (approach 2) to 55% (approach 3), 65% (approach 4) and

finally 78% (approach 5). Nevertheless, increasing the recovery of CPC was correlated with a decrease in CPC purity (**Fig. 5D**), which declined from 4.6 (approach 1) to 2.9 (approach 5). The CPC/APC separation factor decreased for approaches 2-4, but remained above 5, as for the step separation experiments in sections 3.2 and 3.3. In approach 5, where APC was combined with CPC, the APC/CPC separation factor was reduced to 2.9, which was similar to that of the initial FT extract (**Table 1**), and consistent with the observation that all phycobiliproteins loaded were recovered in the same fraction.

These experiments demonstrated that CPC separation using the 3D-printed discs can be tailored for the desired purity and recovery. For example, if high food grade purities are required (i.e., > 2) where APC content is typically not a factor, good recoveries can be achieved with approach 5 [9]. In contrast, higher purities can be targeted for analytical grade CPC using approaches 1 or 2, but at the cost of lower recoveries [10,11]. Furthermore, the 3D-printed discs could be used to recover APC-enriched fractions as an additional high value commercial product [47].

3.5 Impact of 3D-printed chromatographic adsorbers on current chromatography processes

This work has clearly illustrated the potential of 3D-printed adsorbers for the chromatographic separation of phycobiliproteins. The fabricated 3D-printed stationary phases had appropriate macroporous structure for protein separation, and could be operated as traditional chromatography columns. Although the performance of the 3D-printed discs was similar to that of two commercial columns for four different phycobiliprotein-enriched extracts, the 3D-printed discs provided CPC at the highest grade of A620/A280 = 4.2 ± 0.3 (mean ± SD). The elution step optimisations increased the CPC purity to 4.6 at a cost of a *ca*. 10% reduction in total CPC recovery. Compared to the previous 3D-printed gyroid column material [32], the new formulation described here performed better both in terms of CPC recovery and

CPC/APC separation. This opens the possibility for using this formulation to 3D-print more complex column structures such as the Schoen gyroid. Such column morphologies with large printed flow through channels could allow CPC purification directly from diluted crude extracts, which could eliminate the costly and labour-intensive steps of clarification prior to purification [32].

The excellent purification power observed for CPC and APC was obtained with minimal optimisation of the material composition. Fine adjustment of its formulation could lead to improved recovery and purity levels for different phycobiliproteins. Also, the 3D printable material could be specifically adapted to suit other chromatography applications, from ~~AEX~~anion-exchange of other protein targets to the introduction of different chromatographic modes such as cation exchange, hydrophobic interactions, or affinity. It is worth noting that the manufacture of stationary phases through 3D printing is at its early stages, and the resulting chemical, physical and mechanical properties of the monolithic adsorbers are highly dependent on the chemical composition of the parent formulation and the settings employed during 3D-printing. Further investigation is needed to clarify the role of these parameters in the microstructure of the resulting 3D-printed materials, as well as the binding mechanisms between the 3D-printed stationary phase and various biomolecules of interest. However, we believe that using this new material for the fabrication of highly ordered structures will further expand the industrial application of 3D-printed chromatography columns [49]. Notably, the 3D-printed monolithic discs in this work did not include any complex printed bed geometries, as our aim was to compare the performance of the material with commercial products. However, complex bed geometries can be easily fabricated through 3D printing as demonstrated recently [25,32].

4. Conclusions

Here we have characterised for the first time the performance of a directly 3D-printed QA monolithic disc applied for the purification of a complex biological sample, namely phycobiliprotein-enriched extracts from Spirulina. The 3D-printed discs proved to be highly robust and displayed an impressive capacity for chromatographic separation, with up to a 2.9-fold increase in CPC purity. We also demonstrated that CPC separation can be tailored to obtain different levels of purity and recovery. Future investigations will focus on the use of different 3D-printed complex ordered bed structures for the purification of CPC and APC from crude cell extracts, which may be feasible based on the ability to modify pore sizes and architecture while optimising phycobiliprotein binding capacity. This could effectively eliminate steps required to produce high grade CPC and APC that are expensive to scale, such as centrifugation and filtration, as shown in our previous work [32].

CRediT authorship contribution statement

Livia Scorza: Investigation, Data curation, writing – original draft, review & editing. **Ursula Simon**: Investigation, Data curation, writing – review & editing. **Martin Wear**: Resources, methodology. **Alex Zouliatis**: Resources, methodology. **Simone Dimartino**: Funding acquisition, conceptualization, supervision, writing - review & editing. **Alistair McCormick**: Funding acquisition, conceptualization, supervision, writing - review & editing,

Acknowledgements

We thank ScotBio for the Spirulina extracts provided. We also thank BIA Separations for donating the CIM® QA discs. We acknowledge the use of the Cryo FIB/SEM bought with the EPSRC grant EP/P030564/1 and Thomas Glen for help with image acquisition.

Conflict of interest statement

No conflicts, informed consent, or human or animal rights are applicable to this study

Declaration of Competing Interest

The authors declare that they have no known competing financial interests or personal relationships that could have appeared to influence the work reported in this paper.

Funding

LS, SD and AJM acknowledge funding by the Industrial Biotechnology Innovation Centre (IBioIC, grant number 2019-1-1), UK Biotechnology and Biological Sciences Research Council (BB/S020128/1 to AJM) and industrial collaborator ScotBio. US acknowledges the School of Engineering at the University of Edinburgh for her PhD scholarship.

Supplementary material

Supplementary Figure S1. Linear gradient purification of all phycobiliprotein-enriched extracts tested using the HiTrap column. Data are shown for high-shear homogenisation (HS) (A), freezing and thawing (FT) (B), freezing and thawing followed by mixing (FT+M) (C), and freezing and thawing followed by homogenisation (FT+H) (D).

Supplementary Figure S2. Linear gradient purification of all phycobiliprotein extracts tested using the CIM® disc. See **Supplementary Figure S1** for abbreviations.

Supplementary Figure S3. Linear gradient purification of all phycobiliprotein extracts tested using the 3D-printed disc. See **Supplementary Figure S1** for abbreviations.

Supplementary Figure S4. Step purification of all phycobiliprotein extracts tested using the HiTrap column. See **Supplementary Figure S1** for abbreviations.

Supplementary Figure S5. Step purification of all phycobiliprotein extracts tested using the CIM® disc. See **Supplementary Figure S1** for abbreviations.

Supplementary Figure S6. Step purification of all phycobiliproteinextracts tested using a 3D-printed disc. See **Supplementary Figure S1** for abbreviations.

Supplementary Figure S7. Characterisation of purified c-phycocyanin and allophycocyanin extracts. UV-VIS absorption spectra (A) corresponding to HS, FT+M and FT+H phycobiliprotein-enriched extract (grey lines), and CPC- and APC-enriched fractions derived from step separations for each of the three columns (blue and green lines, respectively). SDS-PAGE gels (B) showing separated proteins from CPC- and APC-enriched fractions. The colour legend corresponds to the lines shown in (A). Abbreviations: α APC, alpha subunit of APC; α CPC, alpha subunit of CPC; β APC, beta subunit of APC; β CPC, beta subunit of CPC; FNR, ferredoxin:NADP(+) reductase; LR30 and LR33, c-phycocyanin-associated rod linkers; LRC, phycobilisome rod-core linker.

References

[1] H. Sun, W. Zhao, X. Mao, Y. Li, T. Wu, F. Chen, High-value biomass from microalgae production platforms: Strategies and progress based on carbon metabolism and energy conversion, Biotechnol. Biofuels. 11 (2018) 1–23. https://doi.org/10.1186/s13068-018-1225-6.

[2] J. Singh, D.W. Dhar, Overview of carbon capture technology: Microalgal biorefinery concept and state-of-the-art, Front. Mar. Sci. 6 (2019) 1–9. https://doi.org/10.3389/fmars.2019.00029.

[3] T. Coultate, R.S. Blackburn, Food colorants: their past, present and future, Color. Technol. 134 (2018) 165–186. https://doi.org/10.1111/cote.12334.

[4] M.I. Khan, J.H. Shin, J.D. Kim, The promising future of microalgae: Current status, challenges, and optimization of a sustainable and renewable industry for biofuels, feed, and other products, Microb. Cell Fact. 17 (2018) 1–21. https://doi.org/10.1186/s12934-

018-0879-x.

[5] Persistence Market Research, Microalgae Market : Global Growth & Forecast to 2026, (2018).

[6] S. Khanra, M. Mondal, G. Halder, O.N. Tiwari, K. Gayen, T.K. Bhowmick, Downstream processing of microalgae for pigments, protein and carbohydrate in industrial application: A review, Food Bioprod. Process. 110 (2018) 60–84. https://doi.org/10.1016/j.fbp.2018.02.002.

[7] A. Vonshak, Spirulina platensis (Arthropsira) : physiology, cell-biology and biotechnology, 2002. https://doi.org/10.1007/s13398-014-0173-7.2.

[8] K. Kupferschmidt, In search of blue, Science (80-.). 364 (2019) 424–429. https://doi.org/10.1126/science.364.6439.424.

[9] M. Rito-Palomares, L. Nuez, D. Amador, Practical application of aqueous two-phase systems for the development of a prototype process for c-phycocyanin recovery from Spirulina maxima, J. Chem. Technol. Biotechnol. 76 (2001) 1273–1280. https://doi.org/10.1002/jctb.507.

[10] G. Patil, S. Chethana, A.S. Sridevi, K.S.M.S. Raghavarao, Method to obtain C-phycocyanin of high purity, J. Chromatogr. A. 1127 (2006) 76–81. https://doi.org/10.1016/j.chroma.2006.05.073.

[11] H.L. Wu, G.H. Wang, W.Z. Xiang, T. Li, H. He, Stability and Antioxidant Activity of Food-Grade Phycocyanin Isolated from Spirulina platensis, Int. J. Food Prop. 19 (2016) 2349–2362. https://doi.org/10.1080/10942912.2015.1038564.

[12] Y. Feng, X. Li, Y. Wen, Y. Bu, Method for preparing high purity phycobiliprotein with primary column chromatography, China 200810134122, 2008.

[13] S.T. Silveira, L.K. De Menezes Quines, C.A.V. Burkert, S.J. Kalil, Separation of phycocyanin from Spirulina platensis using ion exchange chromatography, Bioprocess

Biosyst. Eng. 31 (2008) 477–482. https://doi.org/10.1007/s00449-007-0185-1.

[14] D. Kumar, Dolly, W. Dhar, S. Pabbi, N. Kumar, S. Walia, D.W. Dhar, S. Pabbi, N. Kumar, S. Walia, Extraction and purification of C-phycocyanin from Spirulina platensis (CCC540), Indian J. Plant Physiol. 19 (2014) 184–188. https://doi.org/10.1007/s40502-014-0094-7.

[15] I. Deniz, M.O. Ozen, O. Yesil-celiktas, The Journal of Supercritical Fluids Supercritical fluid extraction of phycocyanin and investigation of cytotoxicity on human lung cancer cells, J. Supercrit. Fluids. 108 (2016) 13–18. https://doi.org/10.1016/j.supflu.2015.10.015.

[16] A. Patel, S. Mishra, R. Pawar, P.K. Ghosh, Purification and characterization of C-Phycocyanin from cyanobacterial species of marine and freshwater habitat, Protein Expr. Purif. 40 (2005) 248–255. https://doi.org/10.1016/j.pep.2004.10.028.

[17] S.G. Yan, L.P. Zhu, H.N. Su, X.Y. Zhang, X.L. Chen, B.C. Zhou, Y.Z. Zhang, Single-step chromatography for simultaneous purification of C-phycocyanin and allophycocyanin with high purity and recovery from Spirulina (Arthrospira) platensis, J. Appl. Phycol. 23 (2011) 1–6. https://doi.org/10.1007/s10811-010-9525-7.

[18] A. Ramos, F.G. Acién, J.M. Fernández-Sevilla, C. V. González, R. Bermejo, Development of a process for large-scale purification of C-phycocyanin from Synechocystis aquatilis using expanded bed adsorption chromatography, J. Chromatogr. B Anal. Technol. Biomed. Life Sci. 879 (2011) 511–519. https://doi.org/10.1016/j.jchromb.2011.01.013.

[19] M.I. Khazi, Z. Demirel, F. Liaqat, M.C. Dalay, Analytical grade purification of phycocyanin from cyanobacteria, in: Methods Mol. Biol., 2020: pp. 173–179. https://doi.org/10.1007/7651_2018_202.

[20] J.-F. Niu, G.-C. Wang, X. Lin, B.-C. Zhou, Large-scale recovery of C-phycocyanin

from Spirulina platensis using expanded bed adsorption chromatography, J. Chromatogr. B. 850 (2007) 267–276. https://doi.org/10.1016/j.jchromb.2006.11.043.

[21] S. Oberloier, J. Pearce, General Design Procedure for Free and Open-Source Hardware for Scientific Equipment, Designs. 2 (2017) 2. https://doi.org/10.3390/designs2010002.

[22] S.C. Ligon, R. Liska, J. Stampfl, M. Gurr, R. Mülhaupt, Polymers for 3D Printing and Customized Additive Manufacturing, Chem. Rev. 117 (2017) 10212–10290. https://doi.org/10.1021/acs.chemrev.7b00074.

[23] S. Nawada, S. Dimartino, C. Fee, Dispersion behavior of 3D-printed columns with homogeneous microstructures comprising differing element shapes, Chem. Eng. Sci. 164 (2017) 90–98. https://doi.org/10.1016/j.ces.2017.02.012.

[24] F. Dolamore, C. Fee, S. Dimartino, Modelling ordered packed beds of spheres: The importance of bed orientation and the influence of tortuosity on dispersion, J. Chromatogr. A. 1532 (2018) 150–160. https://doi.org/10.1016/j.chroma.2017.12.004.

[25] M.G. Moleirinho, S. Feast, A.S. Moreira, R.J.S. Silva, P.M. Alves, M.J.T. Carrondo, T. Huber, C. Fee, C. Peixoto, 3D-printed ordered bed structures for chromatographic purification of enveloped and non-enveloped viral particles, Sep. Purif. Technol. 254 (2021) 117681. https://doi.org/10.1016/j.seppur.2020.117681.

[26] C. Fee, S. Nawada, S. Dimartino, 3D printed porous media columns with fine control of column packing morphology, J. Chromatogr. A. 1333 (2014) 18–24. https://doi.org/10.1016/j.chroma.2014.01.043.

[27] V. Gupta, M. Talebi, J. Deverell, S. Sandron, P.N. Nesterenko, B. Heery, F. Thompson, S. Beirne, G.G. Wallace, B. Paull, 3D printed titanium micro-bore columns containing polymer monoliths for reversed-phase liquid chromatography, Anal. Chim. Acta. 910 (2016) 84–94. https://doi.org/10.1016/j.aca.2016.01.012.

[28] S. Sandron, B. Heery, V. Gupta, D.A. Collins, E.P. Nesterenko, P.N. Nesterenko, M. Talebi, S. Beirne, F. Thompson, G.G. Wallace, D. Brabazon, B. Paull, 3D printed metal columns for capillary liquid chromatography, Analyst. 139 (2014) 6343–6347. https://doi.org/10.1039/c4an01476f.

[29] C. Fee, 3D-printed porous bed structures, Curr. Opin. Chem. Eng. 18 (2017) 10–15. https://doi.org/10.1016/j.coche.2017.07.003.

[30] C. Salmean, S. Dimartino, 3D-Printed Stationary Phases with Ordered Morphology: State of the Art and Future Development in Liquid Chromatography, Chromatographia. 82 (2019) 443–463. https://doi.org/10.1007/s10337-018-3671-5.

[31] U. Simon, S. Dimartino, Direct 3D printing of monolithic ion exchange adsorbers, J. Chromatogr. A. 1587 (2019) 119–128. https://doi.org/10.1016/j.chroma.2018.12.017.

[32] U. Simon, L.C.T. Scorza, S. Teworte, A.J. McCormick, S. Dimartino, Demonstration of protein capture and separation using 3D printed anion exchange monoliths fabricated in one-step, J. Sep. Sci. (2020) 0–23. https://doi.org/10.1002/jssc.202000722.

[33] I. İlter, S. Aky, Z. Demirel, M. Koç, M. Conk-dalay, F. Kaymak-Ertekin, Optimization of phycocyanin extraction from Spirulina platensis using different techniques, J. Food Compos. Anal. 70 (2018) 78–88. https://doi.org/10.1016/j.jfca.2018.04.007.

[34] H.A. Tavanandi, R. Mittal, J. Chandrasekhar, K.S.M.S. Raghavarao, Simple and efficient method for extraction of C-Phycocyanin from dry biomass of Arthospira platensis, Algal Res. 31 (2018) 239–251. https://doi.org/10.1016/j.algal.2018.02.008.

[35] S. Chittapun, V. Jonjaroen, K. Khumrangsee, T. Charoenrat, C-phycocyanin extraction from two freshwater cyanobacteria by freeze thaw and pulsed electric field techniques to improve extraction efficiency and purity, Algal Res. 46 (2020) 101789. https://doi.org/10.1016/j.algal.2020.101789.

[36] L.N. Liu, X.L. Chen, Y.Z. Zhang, B.C. Zhou, Characterization, structure and function of linker polypeptides in phycobilisomes of cyanobacteria and red algae: An overview, Biochim. Biophys. Acta - Bioenerg. 1708 (2005) 133–142. https://doi.org/10.1016/j.bbabio.2005.04.001.

[37] A. Bennett, L. Bogorad, Complementary chromatic adaption in a filamentous blue-green alga, J. Cell Biol. 58 (1973) 419–435. https://doi.org/10.1083/jcb.58.2.419.

[38] R.J. Groarke, D. Brabazon, Methacrylate polymer monoliths for separation applications, Materials (Basel). 9 (2016). https://doi.org/10.3390/ma9060446.

[39] E.G. Vlakh, T.B. Tennikova, Preparation of methacrylate monoliths, J. Sep. Sci. 30 (2007) 2801–2813. https://doi.org/10.1002/jssc.200700284.

[40] I. Mihelič, D. Nemec, A. Podgornik, T. Koloini, Pressure drop in CIM disk monolithic columns, J. Chromatogr. A. (2005). https://doi.org/10.1016/j.chroma.2004.10.054.

[41] M.O. Herigstad, S. Dimartino, C. Boi, G.C. Sarti, Experimental characterization of the transport phenomena, adsorption, and elution in a protein A affinity monolithic medium, J. Chromatogr. A. (2015). https://doi.org/10.1016/j.chroma.2015.06.045.

[42] W.K. Chung, A.S. Freed, M.A. Holstein, S.A. McCallum, S.M. Cramer, Evaluation of protein adsorption and preferred binding regions in multimodal chromatography using NMR, Proc. Natl. Acad. Sci. U. S. A. 107 (2010) 16811–16816. https://doi.org/10.1073/pnas.1002347107.

[43] C. Boi, S. Dimartino, S. Hofer, J. Horak, S. Williams, G.C. Sarti, W. Lindner, Influence of different spacer arms on Mimetic Ligand ™ A2P and B14 membranes for human IgG purification, J. Chromatogr. B Anal. Technol. Biomed. Life Sci. 879 (2011) 1633–1640. https://doi.org/10.1016/j.jchromb.2011.03.059.

[44] D.J. Lea-Smith, P. Bombelli, J.S. Dennis, S.A. Scott, A.G. Smith, C.J. Howe, Phycobilisome-deficient strains of synechocystis sp. PCC 6803 have reduced size and

require carbon-limiting conditions to exhibit enhanced productivity, Plant Physiol. 165 (2014) 705–714. https://doi.org/10.1104/pp.114.237206.

[45] I. Eisenberg, D. Harris, Y. Levi-Kalisman, S. Yochelis, A. Shemesh, G. Ben-Nissan, M. Sharon, U. Raviv, N. Adir, N. Keren, Y. Paltiel, Concentration-based self-assembly of phycocyanin, Photosynth. Res. 134 (2017) 39–49. https://doi.org/10.1007/s11120-017-0406-7.

[46] R.R. Sonani, Recent advances in production, purification and applications of phycobiliproteins, World J. Biol. Chem. 7 (2016) 100. https://doi.org/10.4331/wjbc.v7.i1.100.

[47] S. Sekar, M. Chandramohan, Phycobiliproteins as a commodity: Trends in applied research, patents and commercialization, J. Appl. Phycol. 20 (2008) 113–136. https://doi.org/10.1007/s10811-007-9188-1.

[48] GE_Healthcare, Ion Exchange Chromatography & Chromatofocusing - Principles and Methods, GE Healthcare Bio-Sciences AB, Uppsala Sweden, 2004.

[49] C.J. Fee, S. Dimartino, T. Huber, Separation Medium, WO2017103863A1, 2017. https://patents.google.com/patent/WO2017103863A1/pt.

Figure Legends

Figure 1. Representative image of a washed 3D-printed monolithic disc in a green polylactic acid ring (A) and an SEM image of a monolith cross-section after freeze fracture (B). Monolithic discs were printed in 50 µm layers using an energy of 40 mJ/cm^2 for the curing of each layer. The SEM image shows the porous interconnected globular network of the monolith. Abbreviations: SEM, scanning electron microscopy.

Figure 2. Purity and recovery of c-phycocyanin from step elution runs. Chromatographic profiles are shown for one representative phycobiliprotein-enriched extract (freeze and thawing (FT); n=1) using the commercial HiTrap column (A), commercial monolithic disc (CIM®) (B), and 3D-printed disc (C). The chromatographic profiles for all phycobiliprotein-enriched extracts are shown in Supplementary Figures (S1-S6; n=4). The purity of CPC (D), CPC/APC separation factor (E) and recovery of CPC (F) are shown for all phycobiliprotein extract-column combinations (n=4). The data represent all material collected from the CPC elution step (90 mM NaCl for the HiTrap column, 125 mM NaCl for the CIM® disc and 320 mM NaCl for the 3D-printed disc). Abbreviations: APC: allophycocyanin, CPC: c-phycocyanin, FT: freezing and thawing, FT+M: freezing and thawing followed by mixing, FT+H: freezing and thawing followed by homogenisation, HS: high-shear homogenisation.

Figure 3. Characterisation of purified c-phycocyanin and allophycocyanin extracts. UV-VIS absorption spectra (A) corresponding to one representative phycobiliprotein-enriched extract (freeze and thawing (FT); grey line), and CPC- and APC-enriched fractions derived from step separations for each of the three columns (blue and green lines, respectively). A representative SDS-PAGE gel (B) showing separated proteins from CPC- and APC-enriched fractions. The colour legend corresponds to the lines shown in (A). See **Supplementary Fig. S7** for

characterisations of HS, FT+M and FT+H extracts. Abbreviations: α APC: alpha subunit of APC, α CPC: beta subunit of CPC, β APC: beta subunit of APC, β CPC: beta subunit of CPC, APC: allophycocyanin, CPC: c-phycocyanin, FT: freezing and thawing, FT+M: freezing and thawing followed by mixing, FT+H: freezing and thawing followed by homogenisation, HS: high-shear homogenisation, SDS-PAGE: sodium dodecyl sulphate-polyacrylamide gel electrophoresis, UV-VIS: ultraviolet–visible spectrophotometry.

Figure 4. Performance of two different 3D-printed discs in successive separation cycles using the FT phycobiliprotein-enriched extract. Purity of CPC (A), CPC/APC separation factor (B) and recovery of CPC (C). Disc 1 was run for five cycles and disc 2 was run for a total of thirteen cycles (n=18). Abbreviations: APC: allophycocyanin, CPC: c-phycocyanin, FT: freezing and thawing.

Figure 5. Optimisation of CPC recovery using the 3D-printed discs. Step elution was performed with 20 CVs at 200 and 20 CVs at 320 mM NaCl (A), or with 10 CVs at 200 and 20 CVs at 320 mM NaCl (B), or with 10 CVs at 200 and 30 CVs at 320 mM NaCl (C). CPC recovery, purity and CPC/APC separation factors from the different runs (D). Five different data elaboration methods were used to calculate these descriptors as indicated by the blue shaded areas in the chromatograms. Abbreviations: APC: allophycocyanin, CPC: c-phycocyanin, CV: column volume.

Table 1. Properties of clarified phycobiliprotein-enriched Spirulina extracts. Extracts were processed by freezing and thawing (FT), freezing and thawing followed by mixing (FT+M), freezing and thawing followed by homogenisation (FT+H), or high-shear homogenisation (HS). C-phycocyanin (CPC) concentrations represent the diluted extracts (as in section 2.5) measured using an Äkta Pure 25 chromatography system.

Extract	**[CPC]** (mg/ml)	**CPC Purity** (A620/A280)	**CPC/APC** (A620/A652)
FT	0.3	1.6	2.8
FT+M	0.4	1.3	2.7
FT+H	0.4	1.3	2.1
HS	0.1	1.8	2.2

APC: allophycocyanin, CPC: C-phycocyanin, FT: Freezing and thawing, FT+M: freezing and thawing followed by mixing, FT+H: freezing and thawing followed by homogenisation, HS: high-shear homogenisation.

Highlights

- Developed a 3D printing formula to fabricate anion exchange monolithic adsorbers.
- Captured and separated c-phycocyanin and allophycocyanin from Spirulina extracts.
- The elution protocol could be tailored for recovery and purity of c-phycocyanin.
- Separation using 3D-printed discs was similar to or better than commercial columns.
- 3D-printed discs had robust and scalable purification performance for c-phycocyanin.

Graphical Abstract

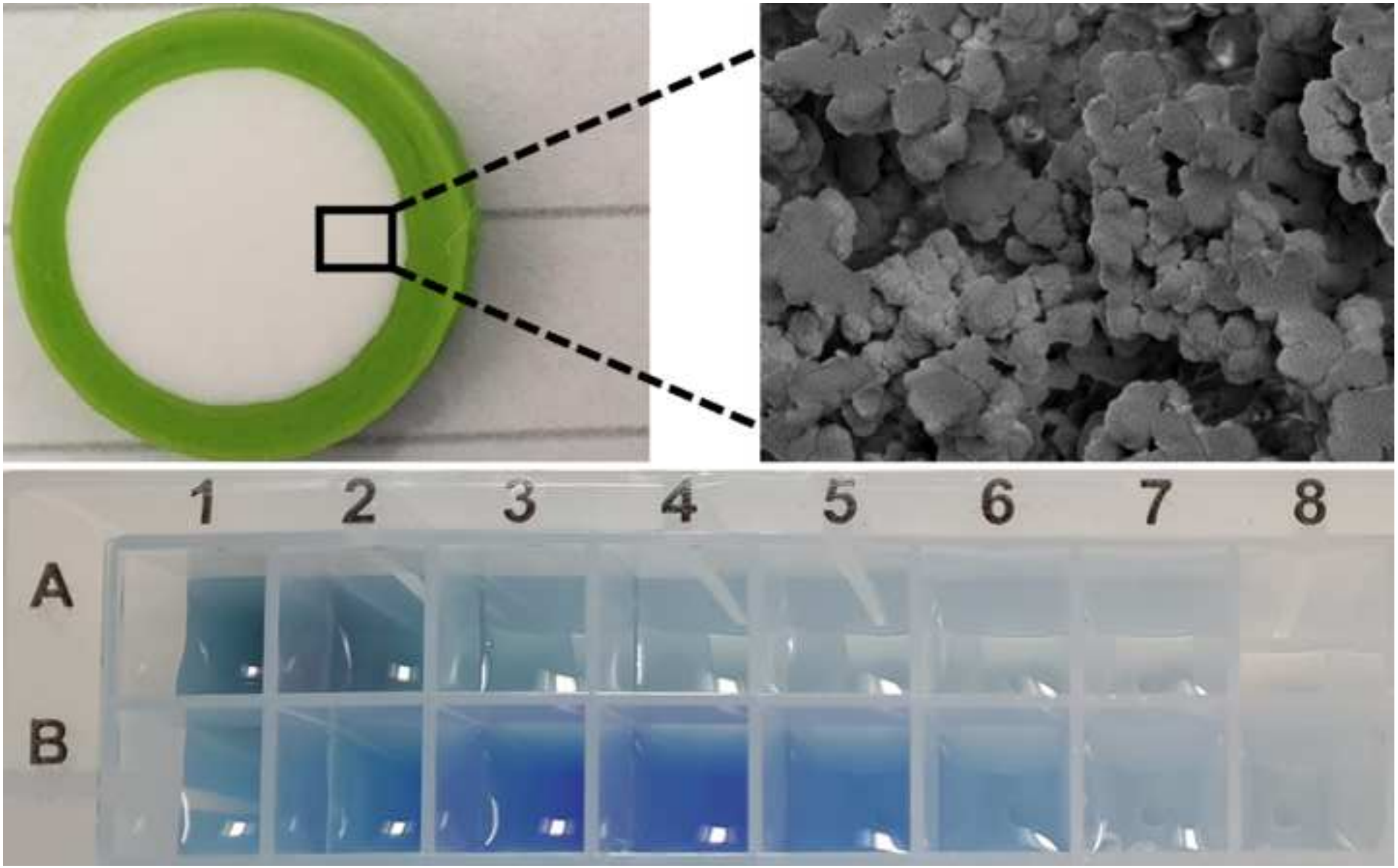

Evaluation of novel 3D-printed monolithic adsorbers against conventional chromatography columns for the purification of c-phycocyanin from Spirulina

Livia C T Scorza[1], Ursula Simon[2], Martin Wear[3], Alex Zouliatis[4], Simone Dimartino[2], Alistair J McCormick[1,†]

[1] SynthSys & Institute of Molecular Plant Sciences, School of Biological Sciences, University of Edinburgh, Edinburgh, EH9 3BF, UK

[2]Institute for Bioengineering, School of Engineering, University of Edinburgh, Edinburgh, EH9 3DW, UK

[3]The Edinburgh Protein Purification Facility, University of Edinburgh, Edinburgh, EH9 3JR, UK

[4]ScotBio, BioCity Scotland, Motherwell, ML1 5UH, UK

[†] Corresponding author

Article type: Research

Authors:	Emails:	ORCID:
Livia C T Scorza	scorza.livia@gmail.com	0000-0002-0145-3592
Ursula Simon	u.simon@ed.ac.uk	
Martin Wear	martin.wear@ed.ac.uk	0000-0003-2208-2986
Alex Zouliatis	alex@scotbio.com	
Simone Dimartino	simone.dimartino@ed.ac.uk	0000-0002-9695-1278
Alistair McCormick	alistair.mccormick@ed.ac.uk	0000-0002-7255-872X

[†]corresponding author:
Dr Alistair J. McCormick
Daniel Rutherford Building, Institute of Molecular Plant Sciences
School of Biological Sciences, University of Edinburgh
The King's Buildings, EH9 3BF Phone: +44 (0)1316505316

Abstract

Extraction and purification of high-grade phycobiliproteins is a multistep process that typically involves costly chromatographic separation techniques. 3D printing approaches and materials can now be tailored to fabricate low-cost anion exchange monolithic adsorbers for chromatography. In this work, a new printing formulation was used to produce monolithic discs with quaternary amine functionality. The 3D-printed discs were tested for the purification of the phycobiliproteins c-phycocyanin and allophycocyanin from extracts of the cyanobacterium *Arthrospira platensis* (Spirulina). Analytical grade c-phycocyanin with 41 ± 7 % recovery was obtained with the 3D-printed discs in a single step. The 3D-printed discs also demonstrated similar or higher separation properties when compared with commercial Q-Sepharose and commercial monolithic discs. Reproducibility tests showed that the fabrication of the 3D-printed discs was robust and potentially scalable for industry-scale purification. Overall, the operative flexibility, robustness and separation performance of the 3D-printed discs demonstrated the promising potential of monolithic adsorbers for the separation of a wide range of biomolecules.

Keywords: allophycocyanin, anion exchange, Arthrospira platensis, disc, downstream processing, phycobilisome.

1. Introduction

Microalgae are a metabolically diverse group of photosynthetic organisms that can be used to sustainably produce commodity biochemicals and sequester carbon dioxide (CO_2) [1,2]. An increasing demand for naturally sourced food additives, cosmetic and health products has driven rapid growth in the microalgal biotechnology industry [3,4], which has a forecasted compound annual growth rate of 4.6% from 2017-2026 [5]. However, optimising downstream processes, including product extraction, purification and yield, remains a key challenge for improving commercial viability [6].

Arthrospira platensis (commonly known as Spirulina) is a cyanobacterial species that has been mass cultivated at large scales with sustained commercial success for several decades [7]. Important products extracted from Spirulina include the blue phycobiliproteins c-phycocyanin (CPC) and allophycocyanin (APC). CPC and APC are both components of the phycobilisome light harvesting complex with absorbance peaks at 620 and 652 nm, respectively. CPC, in particular, is considered a high value product due to the current widespread demand for natural blue colourants [8]. The purity of CPC extracts is typically estimated by spectrophotometry using the ratio of the CPC absorbance peak vs. total protein (i.e., A620/A280) [9]. The purity ratio is generally classified as food grade (A620/A280 > 0.7) up to analytical grade (A620/A280 > 4) [10–12], with the market price of CPC increasing with its purity grade.

Achieving high purities for CPC remains a costly process that involves several processing steps [9]. Cell disruption for crude extraction of phycobiliproteins from Spirulina biomass can be done using a variety of methods, including freezing and thawing, homogenisation [10,13,14], or more expensive approaches such as supercritical CO_2 extraction [15]. Purification of CPC from the crude lysates generally requires appropriate extraction buffers (e.g., in terms of pH and ionic strength), precipitation using ammonium sulphate, followed by dialysis and then one or more chromatography methods, such as expanded bed absorption

chromatography (EBAC), gel filtration or packed bed ion-exchange chromatography [10,12–14,16–19]. Large scale production of concentrated CPC solutions can be achieved with EBAC, but further purification (e.g., using packed bed anion exchange chromatography) is necessary to achieve higher purity ratios (i.e., towards analytical grade) and remove APC [18,20]. Reducing the costs and number of unit operations involved in CPC recovery and purification are important industry goals.

The growing availability of open source resources in the research community has accelerated the 'in-house' manufacture of bespoke scientific equipment and materials at a lower cost and with higher specifications [21]. 3D printing has emerged as an important tool in this process, due to the relatively low costs of 3D printers, the increasing improvements in resolution and robustness, and the wide range of input materials that can be used [22]. Recent work has demonstrated the suitability of 3D printing for the fabrication of chromatography columns, including the creation of stationary phases with precisely ordered structures [23–25], together with column housing, flow distributors and connectors in one single fabrication step [26–28]. 3D printing allows the fabrication of tailored devices for individual separation challenges, which can enhance the purification efficiency and reduce costs compared to standard commercial columns [29]. The wide-ranging potential of 3D-printed chromatography columns has been described in detail in two recent reviews by Salmean and Dimartino [30] and Fee [29]. In particular, 3D printing of anion-exchange chromatography columns has the potential to provide specialised and highly efficient separations at a much reduced cost compared to standard commercial columns [30,31]. However, the technology is currently constrained by the limited availability of 3D printing materials that present suitable ligands for protein adsorption.

Chemical functionality for chromatography (e.g., anion-exchange) can be introduced to 3D printed materials by adding bifunctional monomers bearing in their molecular structure both

the desired chromatographic ligand as well as a chemical group that can undergo polymerisation. Previously, Simon and Dimartino [31] succeeded in 3D-printing quaternary amine (QA) functionalised columns in a single preparation step that demonstrated protein binding capacities in line or exceeding commercial available materials. More recently, Simon et al. [32] have demonstrated the use of a 3D-printed anion-exchange monolithic bed with Schoen gyroid morphology for the purification of CPC from crude Spirulina extracts. Despite the high protein binding capacity of this material, CPC and APC could not be fully resolved as they eluted together.

In this work, monolithic discs with QA functionality were 3D-printed using a novel material formulation based on methacrylates. The material was optimised in terms of chemical stability, which allowed cleaning-in-place procedures with sodium hydroxide (NaOH) to ensure sanitised conditions over consecutive runs. Furthermore, the porous morphology of the material facilitated an increase in mass transfer and column efficiency compared to those previously reported [31,32]. The 3D-printed discs were then tested using step elution experiments for the separation of CPC and APC from clarified phycobiliprotein-enriched Spirulina extracts. Our results were compared against equivalent commercial strong anion-exchange columns also based on the QA functionality, namely a traditionally resin packed Q-Sepharose column and a monolithic CIM® QA disc column. To demonstrate the potential for industry implementation, the robustness of the 3D printing methods and materials were assessed over repeat cycles and for different column batches. Finally, the elution protocol was optimised to improve CPC recovery from this operation.

2. Materials and methods

2.1 Materials

Phenyl bis(2,4,6-trimethylbenzoyl)-phosphine oxide (Omnirad 819, formerly called Irgacure 819) was donated by IGM resins (Waalwijk, The Netherlands). Tinuvin 326 was donated by BASF (Ludwigshafen, Germany). 1-Dodecanol (98%), 2-(Methacryloyloxy)ethyltrimethylammonium chloride 72% aqueous solution), cyclohexanol (98% (v/v)) and ethanol (99.8% (v/v)) were purchased from Fisher Scientific (Waltham, MA, USA). Ethylene glycol dimethacrylate (EDMA, SR206) was donated from Sartomer Europe (Colombes Cedex, France). Analytical grade sodium phosphate (monobasic, dihydrate; $NaH_2PO_4 \cdot 2H_20$) and sodium chloride (NaCl) were purchased from Fisher Scientific (Waltham, MA, USA). All chemicals were used as received.

2.2 Column 3D printing

The material for 3D printing was prepared by dissolving 1 g of the radical photoinitiator Omnirad 819 and 0.1 g of the photoabsorber Tinuvin 326 in a 100 ml mixture of methacrylate monomers (16% (v/v) EDMA, 12% (v/v) [2-methacryloxy)ethyl]trimethylammonium chloride (MAETAC) and 12% (v/v) (Hydroxyethyl)methacrylate (HEMA)) and porogenic solvents (48% (v/v) cyclohexanol and 12% (v/v) 1-dodecanol). All formulations were stored at room temperature (RT) in tubes covered in aluminium foil to prevent spontaneous polymerisation and were ultra-sonicated for 10 min prior to 3D printing.

Monolithic QA discs with a diameter of 12 mm were designed and sliced using Netfabb 2019 (Autodesk, San Rafael, CA, USA). 3D printing was performed using a Solflex 350 digital light processing printer (W2P Engineering, Vienna, Austria) with a UV-LED at 385 nm. All parts were printed with 50 µm layers using an energy of 40 mJ/cm^2 for the curing of each layer. After printing, the discs were cleaned extensively in 99.8% (v/v) ethanol in three consecutive washes on a roller mixer SRT9D (Stuart, Staffordshire, UK). The discs were then stored in 20% (v/v) ethanol until further use. For the separation experiments, the printed discs were

introduced into polylactic acid rings having 12 mm and 15.9 mm inner and outer diameter, respectively and a height of 3 mm (equivalent to a column volume of 340 µl). The polylactic acid rings were separately 3D-printed using a fused deposition modelling (FDM) printer (KLONER3D®140, KLONER3D® - Clevertek s.n.c., Florence, Italy) and employing a 1.75 mm polylactic acid filament from Rigid.Ink (Wetherby, UK).

2.3 Scanning electron microscopy imaging of 3D-printed monoliths

A Zeiss Crossbeam 550 Focused Ion Beam Scanning Electron Microscopy (Jena, Germany) with Quorum Technologies PP3010T preparation system (Laughton, UK) was used to analyse the microscopic structure of the 3D-printed monoliths. Monoliths were frozen in liquid nitrogen, freeze fractured, sublimated at -90°C for 60 min and then platinum sputter coated prior to imaging.

2.4 Phycobiliprotein extracts

Phycobiliprotein-enriched extracts from *Arthrospira platensis* biomass were provided by ScotBio (Scotland, UK). The *A. platensis* culture was initially harvested using 22 µm filtration bags to obtain a wet algal biomass, which was then mixed with water to make a 30% (w/v) biomass solution. Four different methods were then used for cell disruption and phycobiliprotein extraction: 1) high-shear homogenisation (HS), 2) freezing and thawing (FT), 3) freezing and thawing followed by mixing (FT+M), and 4) freezing and thawing followed by homogenisation (FT+H) [20,33–35]. For HS, the biomass solution was subjected to 15 min of high-shear homogenisation at 15,000 rpm using a rotor-stator (T25 Easy Clean, IKA, Germany). Due to the heat generated by rotor-stator, the biomass solution was kept in an ice-bath during high-shear homogenisation. This was followed by 3 hours of low-shear mixing at 200 rpm at room temperature (RT). For FT, FT+M and FT+H the biomass solution underwent

two cycles of freezing (-18°C for 24 hours) and thawing (4°C for 15 hours). For FT+M the solution was mixed for one hour at 200 rpm at RT after the second cycle. For FT+H the solution was homogenised at 15,000 rpm for 15 min in an ice bath after the second cycle. The four extracts were then clarified by two rounds of centrifugation at 9,000 g for 30 min (Multifuge 3 L-R, Thermo Fisher Scientific, USA). The supernatants of the FT, FT+M and FT+H extracts were filtered through 20-25 µm filter paper (Grade 4, Whatman). All extracts were then filtered through a 5 µm polypropylene membrane filter and finally through a 0.8/0.2 dual PES membrane filter (Polycap HD 36 and Polycap TC 36 capsule filters, respectively, GE Healthcare Lifesciences, USA).

2.5 C-phycocyanin purification

An Äkta Pure 25 chromatography system (GE, USA) equipped with a UV monitor for triple wavelength detection was used to quantify components within the clarified extracts, including total extracted protein, CPC and APC at absorbances of 280, 620 and 652 nm, respectively. Prior to loading, the extracts were diluted in 50 mM NaH_2PO_4 (pH 7.0) and then in 25 mM NaH_2PO_4 (pH 7.0) to reduce the ionic strength of the extracts to that of the equilibration buffer (25 mM NaH_2PO_4 and 20 mM NaCl (pH 7.0)) that had a conductivity of *ca*. 4 mS/cm. The dilution factor was the same for all extracts (6-fold dilution). The diluted extracts were filtered one more time through a 0.22 µm syringe filter (Millex-GP, Merck, Germany). The concentration of CPC in each diluted extract is listed in **Table 1**.

The performance of the 3D-printed discs was compared with a commercial Q Sepharose packed column (HiTrap Q HP® 1 ml) (GE, USA) and a commercial monolithic disc (CIM® QA disc, 0.34 ml column volume, BIA Separations, Ajdovščina, Slovenia). Each column type was tested using the four different types of clarified phycobiliprotein extract (n=4 biological replicates each). All chromatography columns were equilibrated with equilibration buffer prior

to sample loading. A loading of 1 mg of CPC per ml of column volume (CV) was fed to the columns, with total load volume adjusted according to CPC concentration and column volume. The columns were then washed with 5 CVs of equilibration buffer, eluted with a linear NaCl gradient (column dependent) and finally washed with 5 CVs of 1 M NaCl solution. As each column type is characterized by its specific binding properties, elution conditions were tuned to enable recovery of the CPC. For the HiTrap column a 25 CV NaCl gradient from 20 to 200 mM was initially employed. A following step elution with 15 CVs of 90 mM and 15 CVs of 120 mM NaCl was carried out to recover CPC and APC, respectively. The CIM® disc was eluted with a 50 CV gradient from 20 to 200 mM NaCl, while step separation was performed with 20 CVs of 125 mM and 20 CVs of 170 mM NaCl for CPC and APC elution, respectively. The 3D-printed discs were eluted with a 50 CV gradient from 20 to 500 mM, with step separation performed with 20 CVs of 200 mM and 20 CVs of 320 mM NaCl for APC and CPC elution, respectively. New unused 3D-printed discs were used for each phycobiliprotein extract (i.e., HS, FT, FT+H and FT+M). All chromatography runs were performed at 8°C and with a flow rate of 1 ml/min for the HiTrap column and 2 ml/min for the monolithic disc columns.

2.6 Robustness of 3D-printed discs for the separation of phycobiliproteins

To test the robustness of the 3D printed discs, in particular the consistency of the separation results over consecutive runs, two unused 3D-printed discs were tested using the phycobiliprotein-enriched FT extract over five and thirteen separation cycles, each consisting of sample load, washing with equilibration buffer, step elution and washing with 1 M NaCl (as described in 2.5).

2.7 CPC purity and concentration calculations

The attributes of the initial phycobiliprotein-enriched extracts and the eluted CPC fractions were calculated based on the absorbance at 280 nm (total protein content), 620 nm (CPC) and 652 nm (APC). For the phycobiliprotein-enriched extracts, each sample was loaded into the Äkta Pure 25 chromatography system, bypassing the column. The UNICORN software (GE, USA) was employed to integrate the peaks and estimate the volume of the eluted fractions. The purity of CPC was calculated using the A620/A280 ratio as in [9]. The separation factor of CPC from APC was calculated as the A620/A652 ratio [36]. CPC recovery was calculated as the ratio of the amount of CPC collected in the eluted fractions with respect to the mass of CPC fed to the columns. The concentration of CPC was estimated as proposed by Bennett and Bogorad [37]:

[CPC] (mg/ml) = [A620 - 0.474 (A652)] / 5.34

2.8 UV-VIS absorption spectrum and SDS-PAGE

To further compare the purity and protein composition of the eluted CPC and APC fractions against the initial clarified phycobiliprotein extracts, the UV-VIS absorption spectra were measured, and SDS-PAGE was performed for the initial extracts and purified fractions from all of the three anion-exchange columns used. Absorption was measured using a NanoDrop 1000 spectrophotometer (Thermo Fisher Scientific, Waltham, MA, USA). Proteins were separated by SDS-PAGE on a Bolt Bis-Tris Plus gel (Invitrogen, Thermo Fisher Scientific, Waltham, MA, USA) and visualised by staining with Coomassie Brilliant Blue R-250 (BioRad, Hercules, CA, USA).

3. Results and discussion

3.1 Fabrication of the 3D-printed discs

Monolithic discs were 3D-printed using an optimised version of our previously reported acrylate-based QA printing materials (**Fig. 1A**) [31,32]. 3D printing materials are comprised of a complex mixture containing monomers and crosslinkers that form the polymeric network, while a photoinitiator and photoabsorber are used to start and control the polymerisation reaction, respectively, during the printing process [22]. To print fully functional stationary phases for anion-exchange chromatography, we introduced porogenic compounds to create pores at the nanometer scale and bifunctional monomers to provide QA ligands. Compared to the previous acrylate-based materials, the new material was solely composed of methacyrylate monomers and crosslinker. This resulted in good alkaline stability that allowed standard cleaning-in-place procedures with 1M NaOH. In addition, the ratio of monomer to crosslinker was tuned to 40:60 to create a more open porous network. The resulting 3D-printed monoliths were similar in size and shape to commercial CIM® discs.

After the printing process, the monoliths were extensively cleaned with ethanol to ensure the removal of uncured monomers, porogens, photoinitiator and photoabsorber. During the washing procedure the monoliths changed in appearance from yellow, directly after printing, to white after several washing steps (**Fig. 1A)**. Successful removal of the introduced porogens was demonstrated using SEM, which showed an interconnected globular network (**Fig. 1B**). This morphology is typical for monoliths fabricated using porogens such as cyclohexanol and dodecanol [38,39]. Flow through pores in the order of 1 µm were estimated using SEM images. This corresponded to a four-fold increase in pore size compared to previous 3D-printed QA materials [32], which indicated better pore accessibility and improved diffusional mass transfer. The porous structure of the 3D-printed monolithic discs was also confirmed by a drop in pressure of 3 ± 0.3 bar at a flow rate of 2 mL/min, which is equivalent to a permeability of 3×10^{-15} m^{-2}. These results are in line with other monolithic materials, such as CIM® discs that have a reported permeability of 6×10^{-15} to 1×10^{-14} m^{-2} [40,41].

To confirm a tight fitting of the 3D-printed monolithic discs within the polylactic acid ring and no leakage at the interface (**Fig. 1A**), we performed residence time distribution experiments using acetone as non-retained tracer. A first moment of $\mu_1 = 0.270 \pm 0.002$ ml was determined for all discs, which demonstrated that the discs had a consistent porous structure and that structural defects had not resulted from the insertion of the discs into the polylactic acid rings. In addition, no fronting due to channelling was observed in the residence time distribution curves, which further confirmed a tight fit of the discs in their polylactic acid casings.

3.2 Comparison of separation and purification of phycobiliproteins

The concentration of CPC, CPC purity and the CPC/APC separation factor for the four phycobiliprotein-enriched extracts are summarised in **Table 1**. Chromatographic runs were performed for all phycobiliprotein extract-column combinations. Separation of CPC and APC was initially carried out with linear NaCl gradients (**Supplementary Fig. S1-S3**). The NaCl concentration at which APC and CPC eluted informed the NaCl concentrations used for subsequent step elution runs (**Supplementary Fig. S4-S6**). For all three columns tested, the flow-through and column wash fractions did not appear to contain significant amounts of APC and CPC. This confirmed that the phycobiliproteins were appropriately adsorbed to all anion-exchange resins, whereas most of the soluble protein content in the extracts was not retained and collected in the flow through.

Overall, CPC and APC eluted at lower NaCl concentrations from the HiTrap column (**Fig. 2A**) than from the two monolithic materials **(Fig. 2B, C**). The commercial CIM® QA monolithic disc required 1.4-fold higher NaCl concentration for the recovery of both APC and CPC, while a 1.6- and 3.5-fold increase was necessary for elution of APC and CPC from the custom 3D-printed discs, respectively. The latter result highlighted the stronger protein binding properties of the new formulation used to make the 3D-printed discs, as the NaCl concentration

required for CPC elution with our previous material was similar to that for CIM® QA discs [32]. Our results also indicated differences in the binding interactions of the two phycobiliproteins with the different stationary phases, with stronger binding to the methacrylate-based monolithic discs than the Sepharose backbone of the HiTrap resin.

Interestingly, both commercial columns eluted CPC first followed by APC, whereas the trend was reversed when using the 3D-printed discs. The adsorption and retention properties of a chromatography column are highly dependent on the binding interactions that biomolecules establish with the stationary phases. The observed elution reversal effect indicated the formation of complex interactions between the phycobiliproteins and the 3D-printed discs, possibly due to a combination of ion-exchange and hydrophobic interactions characteristic of multi-modal chromatography [42]. Interactions with the spacer arm employed to link the ion-exchange moieties to the stationary phase could also have influenced the retention characteristics [43]. For example, a relatively short C2 spacer links the QA moieties to the backbone of the 3D-printed discs due to the chemical structure of the bi-functional MAETAC monomer [31]. Thus, any adsorbed biomolecules would be sterically adjacent to the polymeric backbone, which could facilitate additional weak interactions, such as van der Waals and hydrophobic interactions. In contrast, CIM® discs and the beads used in HiTrap columns are manufactured in a 2-step process, where the backbone is first polymerised and cross-linked, followed by ad-hoc immobilization of the Q ligand. While this production method is longer and more complex, it enables higher flexibility of the resulting chemistry and associated protein-ligand interactions.

For each column type, consistent profiles of APC and CPC elution, CPC purity and recovery were observed for all four extracts showed (**Fig. 2D-F**). This indicated that the different harvest and cell disruption methods had a negligible influence on the following purification steps. Furthermore, similar CPC purities were observed for all three columns, with an average CPC

purity of 3.8 ± 0.3, 3.6 ± 0.1 and 4.2 ± 0.3 (mean ± SD; n=4) for the HiTrap column, CIM® disc and 3D-printed disc, respectively (**Fig. 2D**). This corresponds to a 2.6-fold increase in purity compared to the initial extracts. The CPC purity levels obtained with the 3D-printed discs were typically above 4 (i.e., analytical grade [10,11]). The CPC/APC separation factor was also increased, with an average 2-fold increase for the HiTrap column and a 3-fold increase for both the CIM® disc and 3D-printed disc (**Fig. 2E**). The CPC/APC separation factor was above 6.0 for most of the purified CPC extracts, but for FT+M and FT+H extracts separated with the HiTrap column an average CPC/APC separation factor of 4.0 was achieved. These initial step separation protocols were not optimized for CPC recovery, and co-elution of CPC and APC was observed for all columns, with a significant portion of CPC entering the APC-rich fraction. This resulted in average CPC recoveries of 53 ± 3%, 61 ± 6% and 41 ± 7% (mean ± SD; n=4) for the HiTrap column, CIM® disc and 3D-printed disc, respectively (**Fig. 2F**).

Analyses of the UV-VIS absorbance spectra from each of the purified extracts showed expected peaks at 620 nm and 652 nm for CPC- and APC-enriched fractions, respectively (**Fig. 3A**; **Supplementary Fig. S7A**). All APC fractions also had a peak at 620 nm, as a portion of CPC eluted together with APC in all columns tested (**Fig. 2A-C**). The separation of CPC from APC was further confirmed by SDS-PAGE, where separate bands corresponding to the α- and β-subunits of CPC and APC were visualised (**Fig. 3B**; **Supplementary Fig. S7B**). As observed for absorbance measurements, bands for the subunits of CPC were also present in the APC-enriched fractions, whereas the CPC-enriched fraction did not show any appreciable APC content.

Three hypotheses for the observed co-elution of CPC with APC are summarised below. Firstly, residual CPC may be bound to APC by the phycobilisome rod-core linker protein LRC [36,44]. Although phycobilisome linker proteins (including LRC) were found in the more concentrated phycobiliprotein-enriched extracts, LRC was not observed in the purified extracts

(**Supplementary Fig. S7B**). Secondly, unbound CPC in solution can exist in a variety of oligomeric states of different net charge (i.e., monomers, trimers and hexamers) [45], and thus might elute at different NaCl concentrations resulting in overlap with APC. Thirdly, different binding sites on the monolith surface may lead to the formation of multiple complex interactions with the phycobiliproteins, thus altering the elution pattern during the NaCl gradient.

By appropriate optimisation of the elution protocol, it would be possible to obtain a range of different fractions with each having specific CPC purity and CPC/APC levels for different commercial targets (e.g., food up to analytical grade). Furthermore, APC is a co-product with important added value from this manufacturing process, with commercial potential similar to that of CPC [46]. For example, APC is also considered a high value product and has been used as a fluorescent label and a phycobiliprotein-conjugate in research applications [47].

3.3 Robustness of the fabrication protocol and reproducibility of successive separation cycles with the 3D-printed discs

Validation of the robustness of the manufacturing protocols and consistency of the chromatographic performance are extremely important to enable industry implementation of these new materials in manufacturing operations. To test the reproducibility of the fabrication procedure of the 3D-printed discs, five successive separation cycles were performed with two unused discs using the FT phycobiliprotein-enriched extract. The results for the two discs were comparable to each other and provided a preliminary demonstration of the robustness of the 3D printing protocol and materials employed indicating that the fabrication of the 3D-printed discs was highly consistent.

To test the robustness of the 3D printed monolith over consecutive runs, one disc was tested for a further eight cycles, for a total of thirteen cycles. A minor decline in CPC purity and

recovery was observed from cycle to cycle, with an average decrease of less than 2% per cycle (**Fig. 4A, C**). While this decrease was practically negligible for two adjacent cycles, it was compounded over several subsequent cycles, which led to a drop in purity and recovery of approximately 20% over the 13 cycles performed. CPC purity declined from an initial value of 4.2 to 3.5, while CPC recovery decreased from approximately 40% in the first cycle to 28% in the thirteenth cycle.

The phycobiliprotein extracts contained a complex mixture of proteins, lipids and metabolites. For the two commercial columns, qualitative changes in appearance similar to those seen for the 3D-printed discs were also observed after repeated runs (e.g., green staining and retention of phycobiliproteins and chlorophyll that could not be removed with a 1 M NaCl wash). Notably, we did not attempt to optimise the washing or cleaning stages for separations using the 3D-printed discs. As such, more appropriate column regeneration steps still need to be developed, for example, employing reverse flow and/or using cleaning buffers such as 6 M guanidine hydrochloride, methanol, isopropanol or 1 M NaOH [48]. Results over repeated cycles also suggested that the cleaning-in-place step should be performed after every five cycles for consistent operation (i.e., when the drop in CPC purity and recovery are limited to within 5% with respect to the first cycle).

The CPC/APC separation factor was fairly constant between cycles (7 ± 0.5; mean ± SD; n=18) and always remained above 5 (**Fig. 4B**), which is in line with previously reported values using conventional anion-exchange columns [16,20]. The observed reproducibility of step elution runs over repeated cycles demonstrated the robustness of the 3D-printed monoliths for chromatographic separations, which should help with future implementation in the process industry.

3.4 Optimisation of c-phycocyanin recovery using 3D-printed discs

In the step separations described in sections 3.2 and 3.3, a significant portion of CPC co-eluted together with APC, thus explaining the low recoveries observed in the CPC-rich fractions (**Fig. 2F**). 3D-printed discs displayed a smaller recovery than the commercial columns, which is in line with the observation that APC eluted first (i.e., in the 200 mM NaCl step) when the column still has a relatively large CPC loading. Yet, the majority of APC eluted in the first half of the 200 mM step (**Fig. 2C**), which suggested that the recovery of CPC from the 3D-printed discs could be improved by either adjusting the duration of the elution steps or by pooling different eluted fractions together. To test this hypothesis, unused 3D-printed discs were tested with the FT phycobiliprotein-enriched extract (an arbitrary choice) using five different approaches:

(1) Step elution as in sections 3.2 and 3.3 (i.e., 20 CVs at 200 mM NaCl and 20 CVs at 320 mM NaCl, with CPC collected only from the 320 mM step) (**Fig. 5A**);

(2) Step elution as in (1), but CPC fractions were also collected from the second half of the 200 mM step (**Fig. 5A**);

(3) The length of the 200 mM step was reduced to 10 CVs, while the 320 mM step was kept at 20 CVs. CPC was collected only from the 320 mM step (**Fig. 5B**);

(4) The length of the 200 mM step was reduced to 10 CVs, while the 320 mM step was increased to 30 CVs. CPC was collected only from the 320 mM step (**Fig. 5C**);

(5) The total recovery of CPC was calculated for both steps of the latter experiment. This was equivalent to collecting fractions from both elution steps in the other elution protocols, and equivalent to a single step elution at 320 mM NaCl.

The recovery of CPC in the first approach was 33%. However, recoveries improved in the subsequent approaches from 48% (approach 2) to 55% (approach 3), 65% (approach 4) and finally 78% (approach 5). Nevertheless, increasing the recovery of CPC was correlated with a decrease in CPC purity (**Fig. 5D**), which declined from 4.6 (approach 1) to 2.9 (approach 5).

The CPC/APC separation factor decreased for approaches 2-4, but remained above 5, as for the step separation experiments in sections 3.2 and 3.3. In approach 5, where APC was combined with CPC, the APC/CPC separation factor was reduced to 2.9, which was similar to that of the initial FT extract (**Table 1**), and consistent with the observation that all phycobiliproteins loaded were recovered in the same fraction.

These experiments demonstrated that CPC separation using the 3D-printed discs can be tailored for the desired purity and recovery. For example, if high food grade purities are required (i.e., > 2) where APC content is typically not a factor, good recoveries can be achieved with approach 5 [9]. In contrast, higher purities can be targeted for analytical grade CPC using approaches 1 or 2, but at the cost of lower recoveries [10,11]. Furthermore, the 3D-printed discs could be used to recover APC-enriched fractions as an additional high value commercial product [47].

3.5 Impact of 3D-printed chromatographic adsorbers on current chromatography processes

This work has clearly illustrated the potential of 3D-printed adsorbers for the chromatographic separation of phycobiliproteins. The fabricated 3D-printed stationary phases had appropriate macroporous structure for protein separation, and could be operated as traditional chromatography columns. Although the performance of the 3D-printed discs was similar to that of two commercial columns for four different phycobiliprotein-enriched extracts, the 3D-printed discs provided CPC at the highest grade of A620/A280 = 4.2 ± 0.3 (mean ± SD). The elution step optimisations increased the CPC purity to 4.6 at a cost of a *ca*. 10% reduction in total CPC recovery. Compared to the previous 3D-printed gyroid column material [32], the new formulation described here performed better both in terms of CPC recovery and CPC/APC separation. This opens the possibility for using this formulation to 3D-print more complex column structures such as the Schoen gyroid. Such column morphologies with large

printed flow through channels could allow CPC purification directly from diluted crude extracts, which could eliminate the costly and labour-intensive steps of clarification prior to purification [32].

The excellent purification power observed for CPC and APC was obtained with minimal optimisation of the material composition. Fine adjustment of its formulation could lead to improved recovery and purity levels for different phycobiliproteins. Also, the 3D printable material could be specifically adapted to suit other chromatography applications, from anion-exchange of other protein targets to the introduction of different chromatographic modes such as cation exchange, hydrophobic interactions, or affinity. It is worth noting that the manufacture of stationary phases through 3D printing is at its early stages, and the resulting chemical, physical and mechanical properties of the monolithic adsorbers are highly dependent on the chemical composition of the parent formulation and the settings employed during 3D-printing. Further investigation is needed to clarify the role of these parameters in the microstructure of the resulting 3D-printed materials, as well as the binding mechanisms between the 3D-printed stationary phase and various biomolecules of interest. However, we believe that using this new material for the fabrication of highly ordered structures will further expand the industrial application of 3D-printed chromatography columns [49]. Notably, the 3D-printed monolithic discs in this work did not include any complex printed bed geometries, as our aim was to compare the performance of the material with commercial products. However, complex bed geometries can be easily fabricated through 3D printing as demonstrated recently [25,32].

4. Conclusions

Here we have characterised for the first time the performance of a directly 3D-printed QA monolithic disc applied for the purification of a complex biological sample, namely

phycobiliprotein-enriched extracts from Spirulina. The 3D-printed discs proved to be highly robust and displayed an impressive capacity for chromatographic separation, with up to a 2.9-fold increase in CPC purity. We also demonstrated that CPC separation can be tailored to obtain different levels of purity and recovery. Future investigations will focus on the use of different 3D-printed complex ordered bed structures for the purification of CPC and APC from crude cell extracts, which may be feasible based on the ability to modify pore sizes and architecture while optimising phycobiliprotein binding capacity. This could effectively eliminate steps required to produce high grade CPC and APC that are expensive to scale, such as centrifugation and filtration, as shown in our previous work [32].

CRediT authorship contribution statement

Livia Scorza: Investigation, Data curation, writing – original draft, review & editing. **Ursula Simon**: Investigation, Data curation, writing – review & editing. **Martin Wear**: Resources, methodology. **Alex Zouliatis**: Resources, methodology. **Simone Dimartino**: Funding acquisition, conceptualization, supervision, writing - review & editing. **Alistair McCormick**: Funding acquisition, conceptualization, supervision, writing - review & editing,

Acknowledgements

We thank ScotBio for the Spirulina extracts provided. We also thank BIA Separations for donating the CIM® QA discs. We acknowledge the use of the Cryo FIB/SEM bought with the EPSRC grant EP/P030564/1 and Thomas Glen for help with image acquisition.

Conflict of interest statement

No conflicts, informed consent, or human or animal rights are applicable to this study

Declaration of Competing Interest

The authors declare that they have no known competing financial interests or personal relationships that could have appeared to influence the work reported in this paper.

Funding

LS, SD and AJM acknowledge funding by the Industrial Biotechnology Innovation Centre (IBioIC, grant number 2019-1-1), UK Biotechnology and Biological Sciences Research Council (BB/S020128/1 to AJM) and industrial collaborator ScotBio. US acknowledges the School of Engineering at the University of Edinburgh for her PhD scholarship.

Supplementary material

Supplementary Figure S1. Linear gradient purification of all phycobiliprotein-enriched extracts tested using the HiTrap column. Data are shown for high-shear homogenisation (HS) (A), freezing and thawing (FT) (B), freezing and thawing followed by mixing (FT+M) (C), and freezing and thawing followed by homogenisation (FT+H) (D).

Supplementary Figure S2. Linear gradient purification of all phycobiliprotein extracts tested using the CIM® disc. See **Supplementary Figure S1** for abbreviations.

Supplementary Figure S3. Linear gradient purification of all phycobiliprotein extracts tested using the 3D-printed disc. See **Supplementary Figure S1** for abbreviations.

Supplementary Figure S4. Step purification of all phycobiliprotein extracts tested using the HiTrap column. See **Supplementary Figure S1** for abbreviations.

Supplementary Figure S5. Step purification of all phycobiliprotein extracts tested using the CIM® disc. See **Supplementary Figure S1** for abbreviations.

Supplementary Figure S6. Step purification of all phycobiliproteinextracts tested using a 3D-printed disc. See **Supplementary Figure S1** for abbreviations.

Supplementary Figure S7. Characterisation of purified c-phycocyanin and allophycocyanin extracts. UV-VIS absorption spectra (A) corresponding to HS, FT+M and FT+H phycobiliprotein-enriched extract (grey lines), and CPC- and APC-enriched fractions derived from step separations for each of the three columns (blue and green lines, respectively). SDS-PAGE gels (B) showing separated proteins from CPC- and APC-enriched fractions. The colour legend corresponds to the lines shown in (A). Abbreviations: α APC, alpha subunit of APC; α CPC, alpha subunit of CPC; β APC, beta subunit of APC; β CPC, beta subunit of CPC; FNR, ferredoxin:NADP(+) reductase; LR30 and LR33, c-phycocyanin-associated rod linkers; LRC, phycobilisome rod-core linker.

References

[1] H. Sun, W. Zhao, X. Mao, Y. Li, T. Wu, F. Chen, High-value biomass from microalgae production platforms: Strategies and progress based on carbon metabolism and energy conversion, Biotechnol. Biofuels. 11 (2018) 1–23. https://doi.org/10.1186/s13068-018-1225-6.

[2] J. Singh, D.W. Dhar, Overview of carbon capture technology: Microalgal biorefinery concept and state-of-the-art, Front. Mar. Sci. 6 (2019) 1–9. https://doi.org/10.3389/fmars.2019.00029.

[3] T. Coultate, R.S. Blackburn, Food colorants: their past, present and future, Color. Technol. 134 (2018) 165–186. https://doi.org/10.1111/cote.12334.

[4] M.I. Khan, J.H. Shin, J.D. Kim, The promising future of microalgae: Current status, challenges, and optimization of a sustainable and renewable industry for biofuels, feed, and other products, Microb. Cell Fact. 17 (2018) 1–21. https://doi.org/10.1186/s12934-018-0879-x.

[5] Persistence Market Research, Microalgae Market : Global Growth & Forecast to

2026, (2018).

[6] S. Khanra, M. Mondal, G. Halder, O.N. Tiwari, K. Gayen, T.K. Bhowmick, Downstream processing of microalgae for pigments, protein and carbohydrate in industrial application: A review, Food Bioprod. Process. 110 (2018) 60–84. https://doi.org/10.1016/j.fbp.2018.02.002.

[7] A. Vonshak, Spirulina platensis (Arthropsira) : physiology, cell-biology and biotechnology, 2002. https://doi.org/10.1007/s13398-014-0173-7.2.

[8] K. Kupferschmidt, In search of blue, Science (80-.). 364 (2019) 424–429. https://doi.org/10.1126/science.364.6439.424.

[9] M. Rito-Palomares, L. Nuez, D. Amador, Practical application of aqueous two-phase systems for the development of a prototype process for c-phycocyanin recovery from Spirulina maxima, J. Chem. Technol. Biotechnol. 76 (2001) 1273–1280. https://doi.org/10.1002/jctb.507.

[10] G. Patil, S. Chethana, A.S. Sridevi, K.S.M.S. Raghavarao, Method to obtain C-phycocyanin of high purity, J. Chromatogr. A. 1127 (2006) 76–81. https://doi.org/10.1016/j.chroma.2006.05.073.

[11] H.L. Wu, G.H. Wang, W.Z. Xiang, T. Li, H. He, Stability and Antioxidant Activity of Food-Grade Phycocyanin Isolated from Spirulina platensis, Int. J. Food Prop. 19 (2016) 2349–2362. https://doi.org/10.1080/10942912.2015.1038564.

[12] Y. Feng, X. Li, Y. Wen, Y. Bu, Method for preparing high purity phycobiliprotein with primary column chromatography, China 200810134122, 2008.

[13] S.T. Silveira, L.K. De Menezes Quines, C.A.V. Burkert, S.J. Kalil, Separation of phycocyanin from Spirulina platensis using ion exchange chromatography, Bioprocess Biosyst. Eng. 31 (2008) 477–482. https://doi.org/10.1007/s00449-007-0185-1.

[14] D. Kumar, Dolly, W. Dhar, S. Pabbi, N. Kumar, S. Walia, D.W. Dhar, S. Pabbi, N.

Kumar, S. Walia, Extraction and purification of C-phycocyanin from Spirulina platensis (CCC540), Indian J. Plant Physiol. 19 (2014) 184–188. https://doi.org/10.1007/s40502-014-0094-7.

[15] I. Deniz, M.O. Ozen, O. Yesil-celiktas, The Journal of Supercritical Fluids Supercritical fluid extraction of phycocyanin and investigation of cytotoxicity on human lung cancer cells, J. Supercrit. Fluids. 108 (2016) 13–18. https://doi.org/10.1016/j.supflu.2015.10.015.

[16] A. Patel, S. Mishra, R. Pawar, P.K. Ghosh, Purification and characterization of C-Phycocyanin from cyanobacterial species of marine and freshwater habitat, Protein Expr. Purif. 40 (2005) 248–255. https://doi.org/10.1016/j.pep.2004.10.028.

[17] S.G. Yan, L.P. Zhu, H.N. Su, X.Y. Zhang, X.L. Chen, B.C. Zhou, Y.Z. Zhang, Single-step chromatography for simultaneous purification of C-phycocyanin and allophycocyanin with high purity and recovery from Spirulina (Arthrospira) platensis, J. Appl. Phycol. 23 (2011) 1–6. https://doi.org/10.1007/s10811-010-9525-7.

[18] A. Ramos, F.G. Acién, J.M. Fernández-Sevilla, C. V. González, R. Bermejo, Development of a process for large-scale purification of C-phycocyanin from Synechocystis aquatilis using expanded bed adsorption chromatography, J. Chromatogr. B Anal. Technol. Biomed. Life Sci. 879 (2011) 511–519. https://doi.org/10.1016/j.jchromb.2011.01.013.

[19] M.I. Khazi, Z. Demirel, F. Liaqat, M.C. Dalay, Analytical grade purification of phycocyanin from cyanobacteria, in: Methods Mol. Biol., 2020: pp. 173–179. https://doi.org/10.1007/7651_2018_202.

[20] J.-F. Niu, G.-C. Wang, X. Lin, B.-C. Zhou, Large-scale recovery of C-phycocyanin from Spirulina platensis using expanded bed adsorption chromatography, J. Chromatogr. B. 850 (2007) 267–276. https://doi.org/10.1016/j.jchromb.2006.11.043.

[21] S. Oberloier, J. Pearce, General Design Procedure for Free and Open-Source Hardware for Scientific Equipment, Designs. 2 (2017) 2. https://doi.org/10.3390/designs2010002.

[22] S.C. Ligon, R. Liska, J. Stampfl, M. Gurr, R. Mülhaupt, Polymers for 3D Printing and Customized Additive Manufacturing, Chem. Rev. 117 (2017) 10212–10290. https://doi.org/10.1021/acs.chemrev.7b00074.

[23] S. Nawada, S. Dimartino, C. Fee, Dispersion behavior of 3D-printed columns with homogeneous microstructures comprising differing element shapes, Chem. Eng. Sci. 164 (2017) 90–98. https://doi.org/10.1016/j.ces.2017.02.012.

[24] F. Dolamore, C. Fee, S. Dimartino, Modelling ordered packed beds of spheres: The importance of bed orientation and the influence of tortuosity on dispersion, J. Chromatogr. A. 1532 (2018) 150–160. https://doi.org/10.1016/j.chroma.2017.12.004.

[25] M.G. Moleirinho, S. Feast, A.S. Moreira, R.J.S. Silva, P.M. Alves, M.J.T. Carrondo, T. Huber, C. Fee, C. Peixoto, 3D-printed ordered bed structures for chromatographic purification of enveloped and non-enveloped viral particles, Sep. Purif. Technol. 254 (2021) 117681. https://doi.org/10.1016/j.seppur.2020.117681.

[26] C. Fee, S. Nawada, S. Dimartino, 3D printed porous media columns with fine control of column packing morphology, J. Chromatogr. A. 1333 (2014) 18–24. https://doi.org/10.1016/j.chroma.2014.01.043.

[27] V. Gupta, M. Talebi, J. Deverell, S. Sandron, P.N. Nesterenko, B. Heery, F. Thompson, S. Beirne, G.G. Wallace, B. Paull, 3D printed titanium micro-bore columns containing polymer monoliths for reversed-phase liquid chromatography, Anal. Chim. Acta. 910 (2016) 84–94. https://doi.org/10.1016/j.aca.2016.01.012.

[28] S. Sandron, B. Heery, V. Gupta, D.A. Collins, E.P. Nesterenko, P.N. Nesterenko, M. Talebi, S. Beirne, F. Thompson, G.G. Wallace, D. Brabazon, B. Paull, 3D printed

metal columns for capillary liquid chromatography, Analyst. 139 (2014) 6343–6347. https://doi.org/10.1039/c4an01476f.

[29] C. Fee, 3D-printed porous bed structures, Curr. Opin. Chem. Eng. 18 (2017) 10–15. https://doi.org/10.1016/j.coche.2017.07.003.

[30] C. Salmean, S. Dimartino, 3D-Printed Stationary Phases with Ordered Morphology: State of the Art and Future Development in Liquid Chromatography, Chromatographia. 82 (2019) 443–463. https://doi.org/10.1007/s10337-018-3671-5.

[31] U. Simon, S. Dimartino, Direct 3D printing of monolithic ion exchange adsorbers, J. Chromatogr. A. 1587 (2019) 119–128. https://doi.org/10.1016/j.chroma.2018.12.017.

[32] U. Simon, L.C.T. Scorza, S. Teworte, A.J. McCormick, S. Dimartino, Demonstration of protein capture and separation using 3D printed anion exchange monoliths fabricated in one-step, J. Sep. Sci. (2020) 0–23. https://doi.org/10.1002/jssc.202000722.

[33] I. İlter, S. Aky, Z. Demirel, M. Koç, M. Conk-dalay, F. Kaymak-Ertekin, Optimization of phycocyanin extraction from Spirulina platensis using different techniques, J. Food Compos. Anal. 70 (2018) 78–88. https://doi.org/10.1016/j.jfca.2018.04.007.

[34] H.A. Tavanandi, R. Mittal, J. Chandrasekhar, K.S.M.S. Raghavarao, Simple and efficient method for extraction of C-Phycocyanin from dry biomass of Arthospira platensis, Algal Res. 31 (2018) 239–251. https://doi.org/10.1016/j.algal.2018.02.008.

[35] S. Chittapun, V. Jonjaroen, K. Khumrangsee, T. Charoenrat, C-phycocyanin extraction from two freshwater cyanobacteria by freeze thaw and pulsed electric field techniques to improve extraction efficiency and purity, Algal Res. 46 (2020) 101789. https://doi.org/10.1016/j.algal.2020.101789.

[36] L.N. Liu, X.L. Chen, Y.Z. Zhang, B.C. Zhou, Characterization, structure and function of linker polypeptides in phycobilisomes of cyanobacteria and red algae: An overview,

Biochim. Biophys. Acta - Bioenerg. 1708 (2005) 133–142. https://doi.org/10.1016/j.bbabio.2005.04.001.

[37] A. Bennett, L. Bogorad, Complementary chromatic adaption in a filamentous blue-green alga, J. Cell Biol. 58 (1973) 419–435. https://doi.org/10.1083/jcb.58.2.419.

[38] R.J. Groarke, D. Brabazon, Methacrylate polymer monoliths for separation applications, Materials (Basel). 9 (2016). https://doi.org/10.3390/ma9060446.

[39] E.G. Vlakh, T.B. Tennikova, Preparation of methacrylate monoliths, J. Sep. Sci. 30 (2007) 2801–2813. https://doi.org/10.1002/jssc.200700284.

[40] I. Mihelič, D. Nemec, A. Podgornik, T. Koloini, Pressure drop in CIM disk monolithic columns, J. Chromatogr. A. (2005). https://doi.org/10.1016/j.chroma.2004.10.054.

[41] M.O. Herigstad, S. Dimartino, C. Boi, G.C. Sarti, Experimental characterization of the transport phenomena, adsorption, and elution in a protein A affinity monolithic medium, J. Chromatogr. A. (2015). https://doi.org/10.1016/j.chroma.2015.06.045.

[42] W.K. Chung, A.S. Freed, M.A. Holstein, S.A. McCallum, S.M. Cramer, Evaluation of protein adsorption and preferred binding regions in multimodal chromatography using NMR, Proc. Natl. Acad. Sci. U. S. A. 107 (2010) 16811–16816. https://doi.org/10.1073/pnas.1002347107.

[43] C. Boi, S. Dimartino, S. Hofer, J. Horak, S. Williams, G.C. Sarti, W. Lindner, Influence of different spacer arms on Mimetic Ligand ™ A2P and B14 membranes for human IgG purification, J. Chromatogr. B Anal. Technol. Biomed. Life Sci. 879 (2011) 1633–1640. https://doi.org/10.1016/j.jchromb.2011.03.059.

[44] D.J. Lea-Smith, P. Bombelli, J.S. Dennis, S.A. Scott, A.G. Smith, C.J. Howe, Phycobilisome-deficient strains of synechocystis sp. PCC 6803 have reduced size and require carbon-limiting conditions to exhibit enhanced productivity, Plant Physiol. 165 (2014) 705–714. https://doi.org/10.1104/pp.114.237206.

[45] I. Eisenberg, D. Harris, Y. Levi-Kalisman, S. Yochelis, A. Shemesh, G. Ben-Nissan, M. Sharon, U. Raviv, N. Adir, N. Keren, Y. Paltiel, Concentration-based self-assembly of phycocyanin, Photosynth. Res. 134 (2017) 39–49. https://doi.org/10.1007/s11120-017-0406-7.

[46] R.R. Sonani, Recent advances in production, purification and applications of phycobiliproteins, World J. Biol. Chem. 7 (2016) 100. https://doi.org/10.4331/wjbc.v7.i1.100.

[47] S. Sekar, M. Chandramohan, Phycobiliproteins as a commodity: Trends in applied research, patents and commercialization, J. Appl. Phycol. 20 (2008) 113–136. https://doi.org/10.1007/s10811-007-9188-1.

[48] GE_Healthcare, Ion Exchange Chromatography & Chromatofocusing - Principles and Methods, GE Healthcare Bio-Sciences AB, Uppsala Sweden, 2004.

[49] C.J. Fee, S. Dimartino, T. Huber, Separation Medium, WO2017103863A1, 2017. https://patents.google.com/patent/WO2017103863A1/pt.

Figure Legends

Figure 1. Representative image of a washed 3D-printed monolithic disc in a green polylactic acid ring (A) and an SEM image of a monolith cross-section after freeze fracture (B). Monolithic discs were printed in 50 µm layers using an energy of 40 mJ/cm^2 for the curing of each layer. The SEM image shows the porous interconnected globular network of the monolith. Abbreviations: SEM, scanning electron microscopy.

Figure 2. Purity and recovery of c-phycocyanin from step elution runs. Chromatographic profiles are shown for one representative phycobiliprotein-enriched extract (freeze and thawing (FT); n=1) using the commercial HiTrap column (A), commercial monolithic disc (CIM®) (B), and 3D-printed disc (C). The chromatographic profiles for all phycobiliprotein-enriched extracts are shown in Supplementary Figures (S1-S6; n=4). The purity of CPC (D), CPC/APC separation factor (E) and recovery of CPC (F) are shown for all phycobiliprotein extract-column combinations (n=4). The data represent all material collected from the CPC elution step (90 mM NaCl for the HiTrap column, 125 mM NaCl for the CIM® disc and 320 mM NaCl for the 3D-printed disc). Abbreviations: APC: allophycocyanin, CPC: c-phycocyanin, FT: freezing and thawing, FT+M: freezing and thawing followed by mixing, FT+H: freezing and thawing followed by homogenisation, HS: high-shear homogenisation.

Figure 3. Characterisation of purified c-phycocyanin and allophycocyanin extracts. UV-VIS absorption spectra (A) corresponding to one representative phycobiliprotein-enriched extract (freeze and thawing (FT); grey line), and CPC- and APC-enriched fractions derived from step separations for each of the three columns (blue and green lines, respectively). A representative SDS-PAGE gel (B) showing separated proteins from CPC- and APC-enriched fractions. The colour legend corresponds to the lines shown in (A). See **Supplementary Fig. S7** for

characterisations of HS, FT+M and FT+H extracts. Abbreviations: α APC: alpha subunit of APC, α CPC: beta subunit of CPC, β APC: beta subunit of APC, β CPC: beta subunit of CPC, APC: allophycocyanin, CPC: c-phycocyanin, FT: freezing and thawing, FT+M: freezing and thawing followed by mixing, FT+H: freezing and thawing followed by homogenisation, HS: high-shear homogenisation, SDS-PAGE: sodium dodecyl sulphate-polyacrylamide gel electrophoresis, UV-VIS: ultraviolet–visible spectrophotometry.

Figure 4. Performance of two different 3D-printed discs in successive separation cycles using the FT phycobiliprotein-enriched extract. Purity of CPC (A), CPC/APC separation factor (B) and recovery of CPC (C). Disc 1 was run for five cycles and disc 2 was run for a total of thirteen cycles (n=18). Abbreviations: APC: allophycocyanin, CPC: c-phycocyanin, FT: freezing and thawing.

Figure 5. Optimisation of CPC recovery using the 3D-printed discs. Step elution was performed with 20 CVs at 200 and 20 CVs at 320 mM NaCl (A), or with 10 CVs at 200 and 20 CVs at 320 mM NaCl (B), or with 10 CVs at 200 and 30 CVs at 320 mM NaCl (C). CPC recovery, purity and CPC/APC separation factors from the different runs (D). Five different data elaboration methods were used to calculate these descriptors as indicated by the blue shaded areas in the chromatograms. Abbreviations: APC: allophycocyanin, CPC: c-phycocyanin, CV: column volume.

Table 1. Properties of clarified phycobiliprotein-enriched Spirulina extracts. Extracts were processed by freezing and thawing (FT), freezing and thawing followed by mixing (FT+M), freezing and thawing followed by homogenisation (FT+H), or high-shear homogenisation (HS). C-phycocyanin (CPC) concentrations represent the diluted extracts (as in section 2.5) measured using an Äkta Pure 25 chromatography system.

Extract	[CPC] (mg/ml)	CPC Purity (A620/A280)	CPC/APC (A620/A652)
FT	0.3	1.6	2.8
FT+M	0.4	1.3	2.7
FT+H	0.4	1.3	2.1
HS	0.1	1.8	2.2

APC: allophycocyanin, CPC: C-phycocyanin, FT: Freezing and thawing, FT+M: freezing and thawing followed by mixing, FT+H: freezing and thawing followed by homogenisation, HS: high-shear homogenisation.

Figure 1

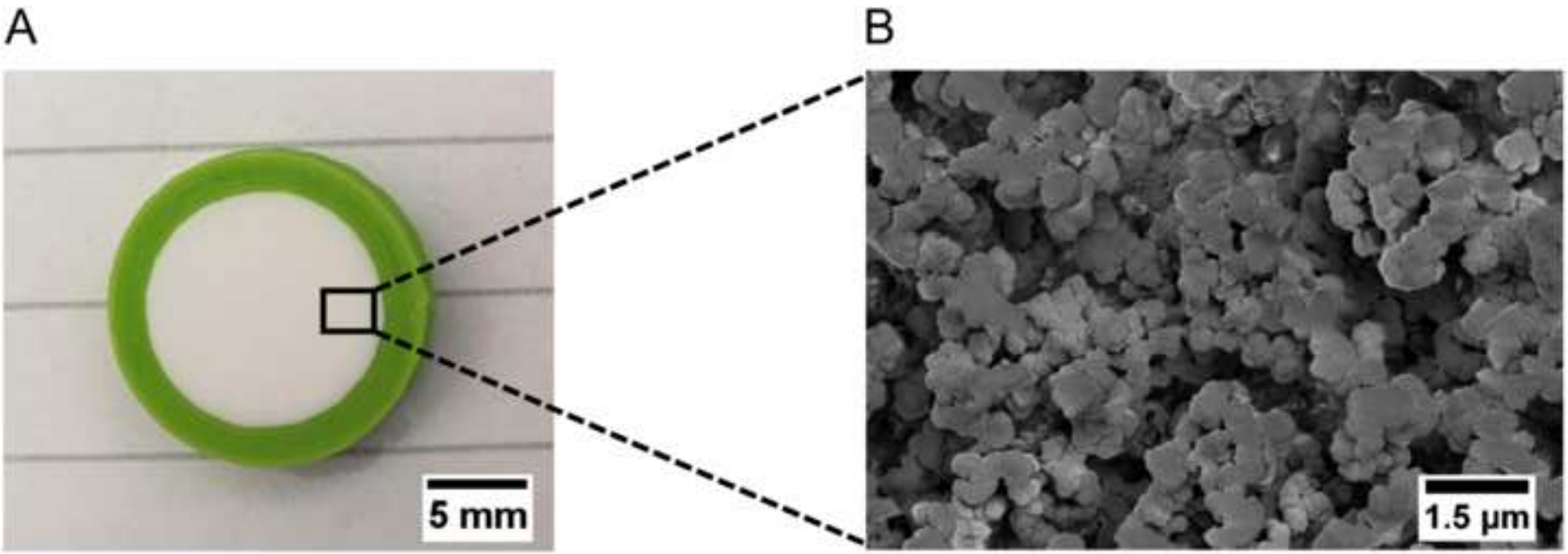

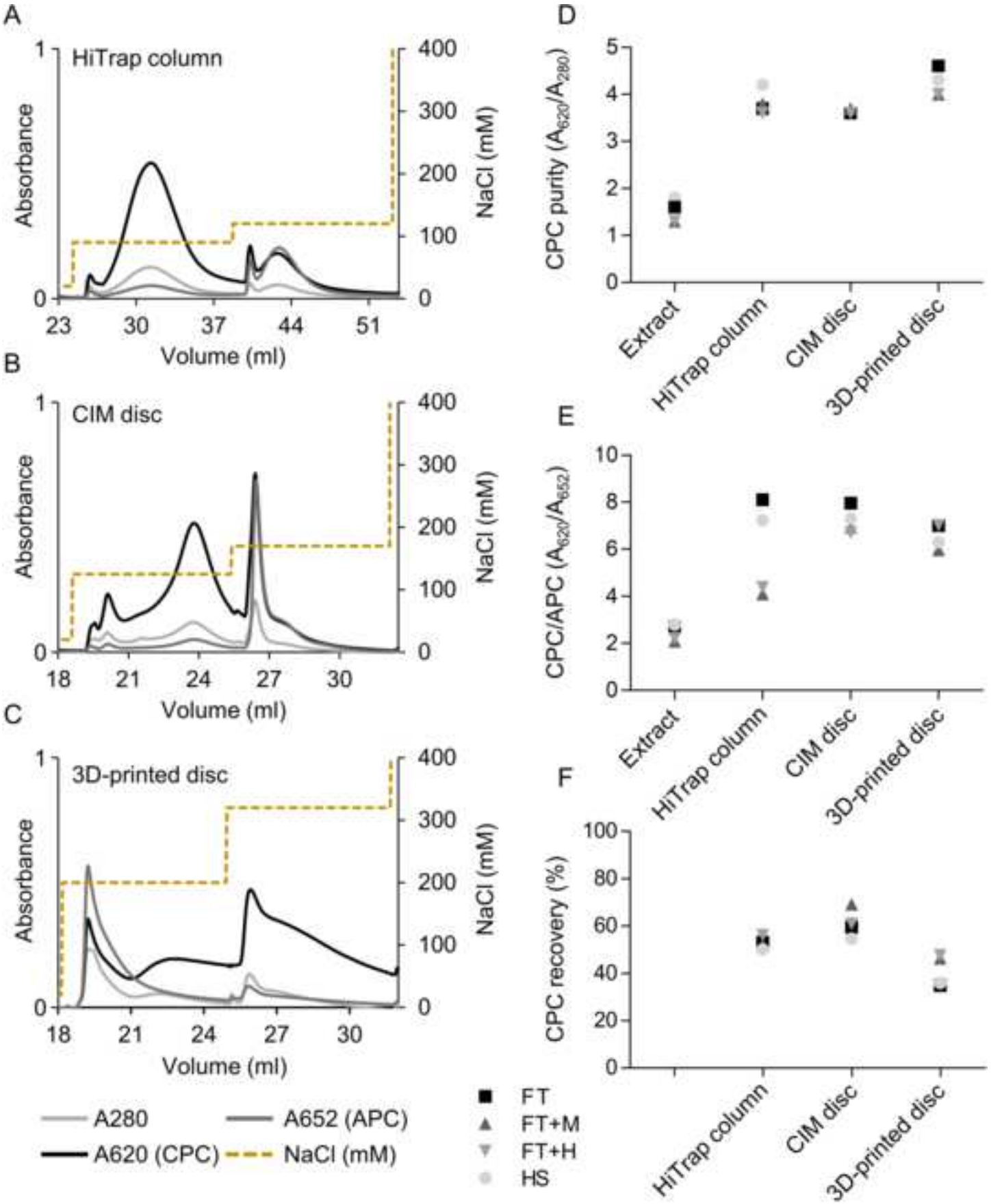

Figure 3 - modified

Click here to access/download;Figure;Slide3 alt.TIF

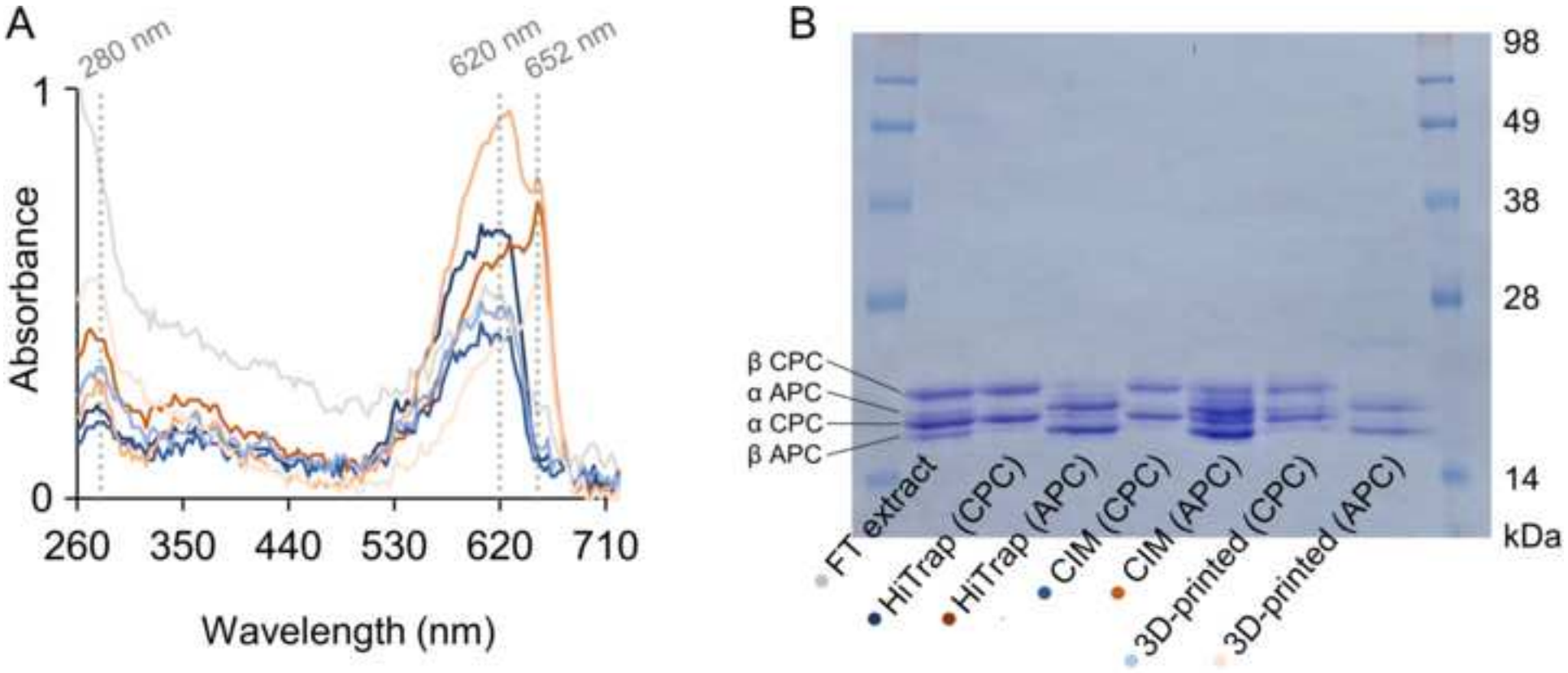

Figure 4

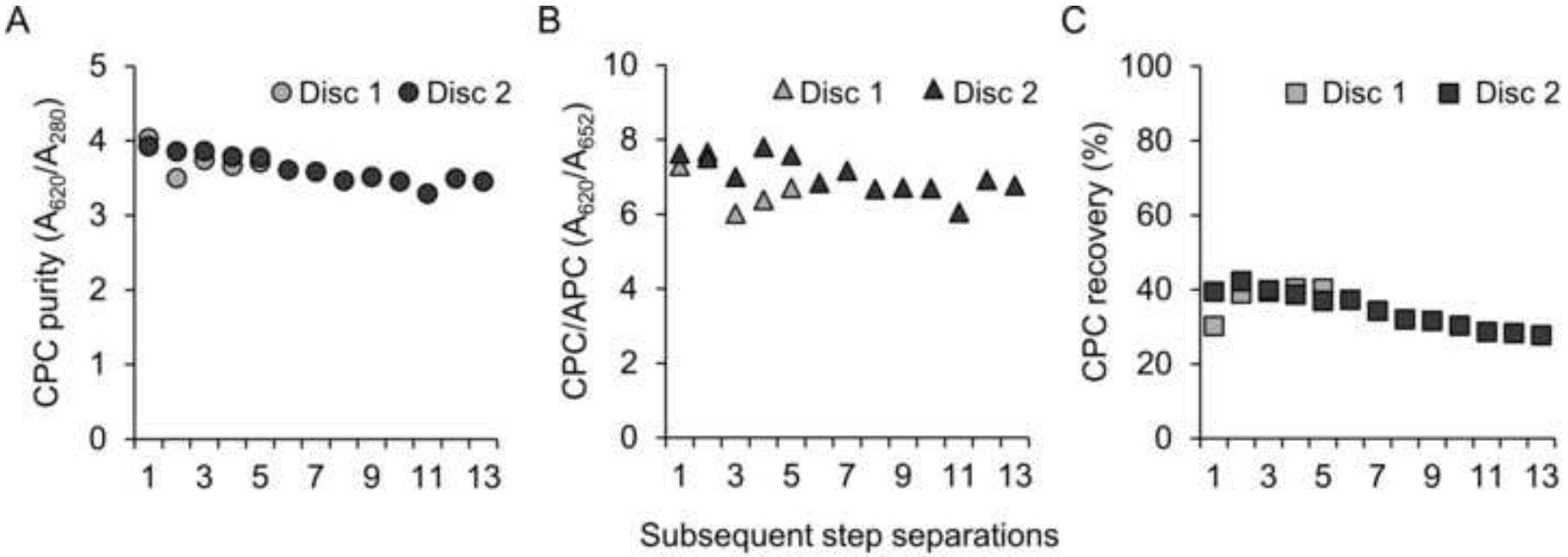

Figure 5

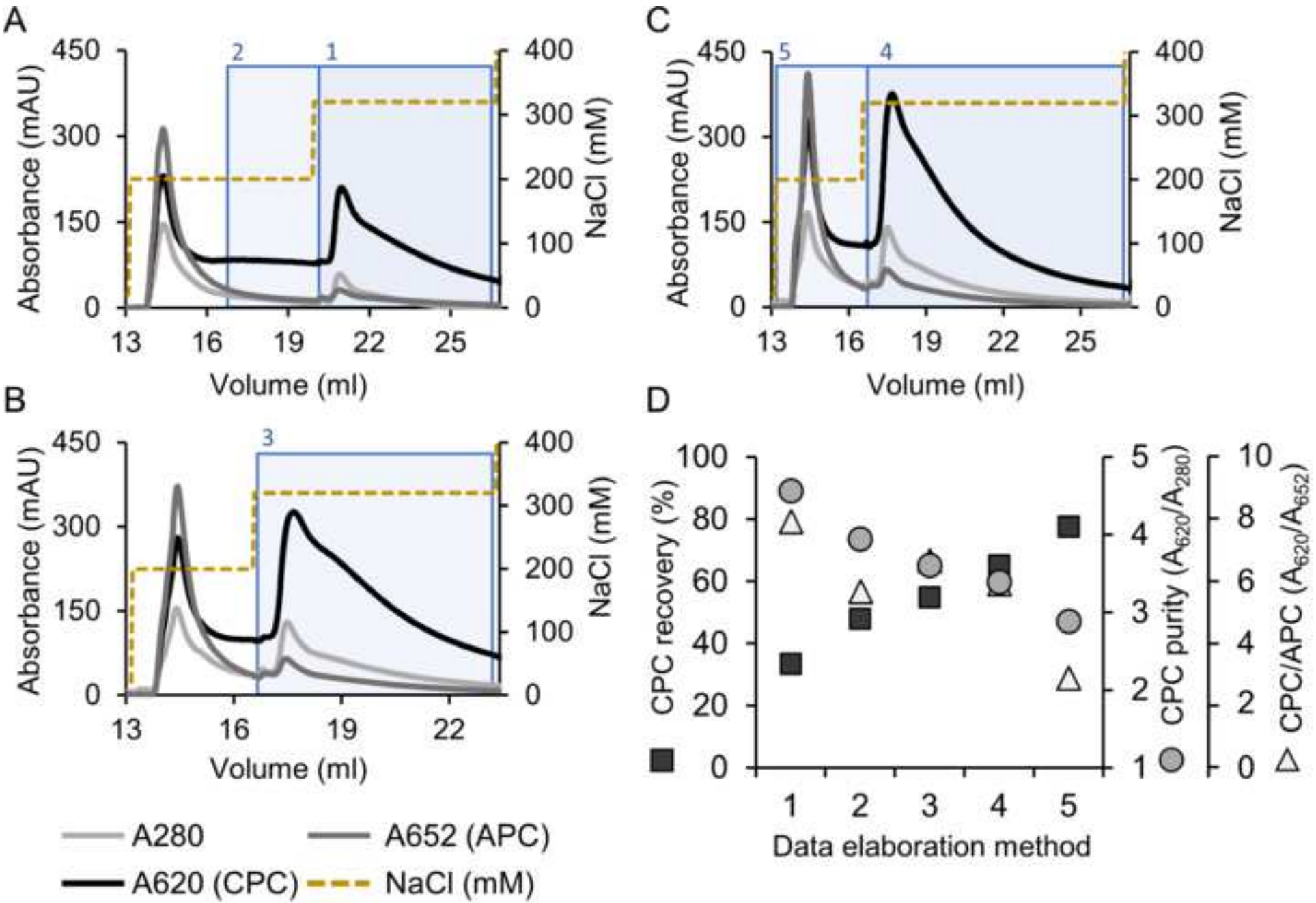

Conflict of interest statement

Declaration of interests

☒ The authors declare that they have no known competing financial interests or personal relationships that could have appeared to influence the work reported in this paper.

☐The authors declare the following financial interests/personal relationships which may be considered as potential competing interests:

CRediT authorship contribution statement

Livia Scorza: Investigation, Data curation, writing – original draft, review & editing. **Ursula Simon**: Investigation, Data curation, writing – review & editing. **Martin Wear**: Resources, methodology. **Alex Zouliatis**: Resources, methodology. **Simone Dimartino**: Funding acquisition, conceptualization, supervision, writing - review & editing. **Alistair McCormick**: Funding acquisition, conceptualization, supervision, writing - review & editing,